# ABSTRACT

Title of Thesis: MESOSCALE EDDIES INFLUENCE ZOOPLANKTON DISTRIBUTION AND GRAZING IN THE GULF OF MEXICO

William August Atkinson II, Master of Science, 2024

Thesis Directed By: Professor Victoria J. Coles, Horn Point Laboratory, University of Maryland Center for Environmental Science

Carbon biomass and net primary productivity, for two size classes of phytoplankton in the Gulf of Mexico (GoM), are calculated from ocean color remote sensing data. Combining these estimates with mechanistic ecosystem model equations allows for analysis of how changes in phytoplankton biomass and community structure propagate through the food web to zooplankton. Biomass and grazing rates are calculated for three size classes of zooplankton (small, large, and predatory) by solving equations from the NEMURO model describing the growth of small and large phytoplankton and zooplankton using the remote sensing net primary productivity, biomass, temperature, and mixed layer depth. The ecosystem model and approach are validated for the GoM and used to assess error propagation. An eddy detection algorithm, tuned for the GoM, is used to calculate the phytoplankton and zooplankton biomass within eddy centers, around eddy edges, and in the immediate surroundings of the eddy to determine the impact of cyclonic and anticyclonic eddies and submesoscale edge effects on patterns of trophic transfer variability. Cyclonic eddy centers increase biomass and anticyclonic eddy centers

decrease biomass in the oligotrophic GoM. Eddy edges contribute to variability in biomass but to a lesser extent than eddy centers. Zooplankton grazing varies in a similar pattern as biomass, and in this oligotrophic region, most grazing is on the largest size class of prey available. Nutrient injection stimulated by eddy dynamics more strongly projects onto biomass in zooplankton trophic levels and their associated grazing which suggests many eddies in the oligotrophic GoM experience top-down control. An understanding of mesoscale eddy impacts on zooplankton dynamics may explain variations in larval fish growth. Advances in remote sensing that allow the discrimination of phytoplankton functional types, such as the new PACE satellite, will be useful for providing a more complete base of the food web and thus enhance estimation of zooplankton biomass.

# MESOSCALE EDDIES INFLUENCE ZOOPLANKTON DISTRIBUTION AND GRAZING IN THE GULF OF MEXICO

by

William August Atkinson II

Thesis submitted to the Faculty of the Graduate School of the
University of Maryland, College Park, in partial fulfillment
of the requirements for the degree of
Master of Science
2024

Advisory Committee:
Professor Victoria J. Coles, Chair
Assistant Research Professor Gregory Silsbe
Associate Professor James Pierson
Professor Kenneth Rose

# Dedication

This thesis is dedicated to my parents, Kim, and William Atkinson. Without their support, I would have never been able to accomplish my academic and career goals. From elementary school to now, they have pushed me to get an education and give 100% into everything I do in life. As a first-generation student, the path was not clear for me to go to college, but my parents put me on the right path to create a better future for my family.

# Acknowledgements

This thesis is the product of the collaboration and support of numerous people and groups. I want to express thanks to the following:

My advisor, Dr. Victoria J. Coles, provided me with this life-changing opportunity and supported me not only in my academic life but my personal life as well. My committee members, Dr. Greg Silsbe, Dr. Jamie Pearson, and Dr. Kenny Rose, for their expertise and providing data which made this research possible. Dr. Taylor Shropshire and Dr. Mike Stukel for their previous work on the NEMURO-GoM model for the Gulf of Mexico. Dr. Raleigh Hood and Marshall Grossman for their advice during lab meetings. Everyone at UMCES and Horn Point Laboratory for providing a safe and fulfilling learning environment in which I was able to thrive and accomplish my goals.

I would also like to thank NASA and the Zooplankton from Space grant for funding this research and making this work possible. Finally, Id like to thank all contributors to the Zooplankton from Space project for their contributions to this research.

# Table of Contents

## Contents

# Chapter 1: Introduction to zooplankton and physical dynamics in the Gulf of Mexico

The Gulf of Mexico (GoM) is a semi-enclosed basin in which the physical dynamics are dominated by the Loop Current and mesoscale and submesoscale eddies (Le Hénaff et al., 2012a; Meunier et al., 2018). The Loop Current is part of the North Atlantic western boundary current system bringing warm water into the GoM through the Yucatan Channel and leaving through the Straits of Florida. It can be identified by warmer than average sea surface temperatures and extends towards the Mississippi, Alabama, and Florida Shelves (MAFLA Shelf). Large anticyclonic (clockwise) eddies occasionally pinch off the Loop Current and propagate westward through the GoM (Hiron et al., 2022). Anticyclonic eddies rotate around high pressure and are characterized as having higher sea surface height (SSH) and sea surface temperature (SST) in their centers. Convergence occurs within their centers causing downwelling of warm surface water. In contrast, cyclonic eddies rotate around low pressure and are characterized as having lower SSH and SST. Divergence occurs within cyclonic eddy centers causing upwelling of cold, nutrient rich sea water (Brokaw et al., 2020). The Bay of Campeche in southwest GoM has a separate cyclonic circulation independent from the Loop Current. The Campeche Gyre can be impacted by Loop Current eddies (anticyclones) which can decrease its vorticity. Alternately, cyclonic eddies accompanied by anticyclonic eddies (dipoles) can strength the Campeche Gyre (Olvera-Prado et al., 2023). Eddies in the oligotrophic GoM can influence production along the continental shelf. Anticyclonic eddies close to the shelf in the western GoM can increase cross-shelf exchange depending on its shape, and proximity to the shelf break. Enhancement can occur at the northern edge of the anticyclonic eddy or southern edge depending on its interaction with

the Campeche Gyre. Eddies near the shelf break can increase transport between the western and eastern GoM (Guerrero et al., 2020).

Zooplankton serve as a crucial link between primary producers and higher trophic levels because they feed on phytoplankton and sometimes other zooplankton and are grazed by fish and fish larvae. The GoM has a diverse zooplankton community structure and differs depending on the specific region of the GoM. In the southern GoM, 16 zooplankton taxonomic groups were found and were dominated by Copepoda, Trematoda, Bivalvia, and Chaetognatha (Cruz-Rosado et al., 2020). The Bay of Campeche region has been characterized as having higher zooplankton biomass even in deepwater due to river discharge and eddy activity in this region (Martinez et al., 2021). The open ocean GoM is often described as being oligotrophic. However, there can be areas with increased zooplankton biomass based on enhancement of nutrient availability. These areas in the oligotrophic GoM can be impacted by eddies resulting in localized highly productive regions (Biggs & Ressler, 2001). In the deepwater region of the GoM, Arthropoda are the dominant phyla while Cnidaria, Chordata and Chaetognatha are also abundant (Martinez et al., 2021). In the northern GoM, Copepods are the most abundant and dominated by the genus *Acartia*. Larger species of zooplankton are associated with more hypoxic conditions and the rarer species are more abundant at increased salinity and decreased temperature (Elliott et al., 2012).

# Chapter 2: Mesoscale eddies influence zooplankton distribution and grazing in the Gulf of Mexico

## *Introduction*

The Gulf of Mexico (GoM) is a semi-enclosed basin in which the physical dynamics are dominated by the Loop Current and mesoscale and submesoscale eddies (Le Hénaff et al., 2012b; Meunier et al., 2018). Anticyclonic eddies rotate clockwise around high pressure which in the spin up phase causes convergence in the center of anticyclonic eddies and downwelling of warm surface water, leading to a depression of the pycnocline in the center of the eddy. In contrast, cyclonic eddies, which are mainly formed within the GoM, rotate counterclockwise around low pressure, and exhibit below average sea surface temperatures and lower sea surface height compared to the water surrounding the eddy due to geostrophic adjustment of the subsurface density field. This causes divergence in the center and upwelling of cold, nutrient rich water during the formation stages (Brokaw et al., 2020), and an elevated pycnocline in the eddy center during the eddy lifetime. Upwelling and downwelling potentially lead to enhanced vertical fluxes of nutrients into and out of the euphotic zone, possibly enhancing primary production and phytoplankton biomass in cyclonic eddies compared to anticyclonic eddies (Gower et al., 1980; Pingree et al., 1979). Factors that might influence these differences potentially include the depth of the nutricline, the intensity of the eddy circulation which dictates the degree of uplift of the subsurface density field and nutricline, and the depth of the light penetration (euphotic zone) in the eddy (McGillicuddy, 2016). Because eddies have been shown to influence primary production and chlorophyll concentration in other regions (Franks et al., 1986; Gaube et al., 2014; Liu & Levine, 2016) as well as the GoM (Damien et al., 2021; Nacional et al., 2002; Toner

et al., 2003), we anticipate that they may also influence zooplankton biomass and trophic transfer in the GoM.

The physical dynamics of both cyclonic and anticyclonic eddies may differ around their edges compared to the center (Samuelsen et al., 2012; Wang et al., 2018; Zhang & Qiu, 2018). Submesoscale processes at the edges of eddies can result in variations in productivity due to the formation of ageostrophic vertical velocities which cause mixing between surface and deeper water (Mahadevan, 2016). Along the edges in both eddy types, there may be enhancement or dilution of plankton biomass depending on whether mixing leads to dilution of a surface intensified biomass peak or drives a biomass enhancement from entrainment of deeper nutrients, or both in sequence. Vertical velocities in eddy edges can also occur due to wind – current interacting effects (Gaube et al., 2013; Mahadevan et al., 2008; McGillicuddy et al., 2007).

While eddies have been shown to affect phytoplankton biomass and community composition (Carvalho et al., 2019; Li et al., 2022; Sánchez-Mejiá et al., 2020; Selph et al., 2022), and while frontal dynamics in phytoplankton have been shown to influence zooplankton and fish behaviors (Biggs & Ressler, 2001; Schmid et al., 2020; Shropshire et al., 2022; Wormuth et al., 2000), the lack of spatially explicit data for zooplankton biomass and grazing has led to only limited local investigations about how zooplankton influence trophic transfer at these spatial scales (Stukel et al., 2011). With existing technologies, there may never be enough in-situ zooplankton observations to compare mesoscale eddy effects on zooplankton throughout the entire GoM.

However, models provide an opportunity to investigate the spatial patterns in zooplankton, particularly when validated with existing observations. Models are subject to their own physical and ecological errors, but they provide a self-consistent solution that merges

zooplankton and phytoplankton dynamics. The proposed method reduces the physical errors introduced by model error and biases by using observed remote sensing data as the base inputs for biological model equations that provide spatial and temporal resolution of key coupling between primary producers and zooplankton. Remotely sensed variables such as temperature and phytoplankton carbon biomass are input into mechanistic model equations to provide high spatial and temporal resolution estimates of zooplankton biomass. While this method requires an equilibrium assumption, the solution changes daily in time with new input fields, allowing us to relate biomass and physical dynamics across time and space.

There is significant cloud cover in the GoM which reduces the remotely sensed data availability. Therefore, we use a census approach, aggregating all the eddies over a 4-year period (2003-2006) to address the following objectives:

1. Analyze the impact on the food web between anticyclonic and cyclonic eddies.

2. Evaluate the role of eddy centers in influencing zooplankton biomass and grazing rates throughout the GoM.

3. Investigate the physical dynamics occurring at the edge of GoM eddies and how the edges impact trophic transfer in the GoM.

We first describe the temporal and spatial patterns in eddies and zooplankton biomass. We then analyze the differences between the anticyclonic and cyclonic eddy centers and their role on the food web. We then investigate the impacts on the food web of the physical dynamics occurring along eddy edges.

## *Data and Methods*

### Physical-biogeochemical model

An existing, validated coupled physical-biogeochemical model (Shropshire et al., 2020) is used both as the basis and validation for our zooplankton estimates. The North Pacific Ecosystem Model for Understanding Regional Oceanography (NEMURO) was originally developed for the North Pacific but has been re-parametrized and validated to reflect the physical dynamics of the Gulf of Mexico using both historical and new observations (NEMURO-GoM) (Shropshire et al., 2020). NEMURO is an ecosystem model that describes the relationships among trophic levels across a range of size classes and is thus well suited to describe trophic transfer dynamics in this region. The model predicts, two size classes of phytoplankton (small and large P) and three size classes of zooplankton (small, large, and predatory Z) (Kishi et al., 2007). Small phytoplankton represent picophytoplankton like Prochlorococcus and cyanobacteria while large phytoplankton represent microphytoplankton or heterotrophic protists like flagellates, ciliates, and diatoms. Small zooplankton represent heterotrophic nanoflagellates, large zooplankton represent suspension feeding mesozooplankton like copepods in the genus *Acartia*, and predatory zooplankton represent metazoan predatory zooplankton like Chaetognaths or copepods such as *Euchaeta* spp. The NEMURO-GoM biogeochemical model was imbedded in a physical Hybrid Coordinate Ocean Model (HYCOM) model (Chassignet et al., 2003) which has a spatial resolution of about 4 kilometers (Shropshire et al., 2020). We used HYCOM model version (expt50.1, https://www.hycom.org/data/gomu0pt04/expt-50pt1) which assimilates satellite altimeter observations, satellite and in-situ SST observation and vertical temperature and salinity profiles from Argo floats. We used sea surface height anomaly (SSH) from the data assimilating model for obtaining estimates of both anticyclonic and cyclonic eddies. Mixed layer

depth from the data assimilation model was used for estimation of the vertically integrated net primary production (NPP).

**Estimating zooplankton biomass and grazing**

The NEMURO-GoM model consists of mechanistic equations describing the changes in small and large phytoplankton and small, large, and predatory zooplankton biomass resulting from growth and mortality. The zooplankton grazing terms represent one form of mortality for the phytoplankton groups. Satellite derived fields of temperature, phytoplankton biomass and its partitioning between large and small groups, and NPP are integrated over the mixed layer depth from HYCOM. Assuming that the rate of change in biomass is small, the phytoplankton equations from the model can be used to estimate zooplankton and grazing in the Gulf of Mexico (Coles, Atkinson, Huebert, Pierson, Rose, Chaichitehrani, in prep). The method was applied to fields from the model to assess the skill of the method (Zs correlation .91 and rmse .013, Zl correlation and rmse .016 .71, Zp correlation .78 and rmse .012). We apply this technique to remote sensing data in the Gulf of Mexico to better understand the role of eddies in driving trophic transfer and spatial heterogeneity.

**Remote sensing data**

The satellite data products used in this research include sea surface temperature (SST) as well as estimates of phytoplankton carbon biomass, size fractionation, and NPP. Biological fields originated from the Moderate Resolution Imaging Spectroradiometer (MODIS) instrument on board the NASA Aqua satellite. Daily fields of chlorophyll-a (Chl a), sea surface temperature (SST), phytoplankton carbon biomass and photosynthetic active radiation (PAR) were obtained from the NASA Ocean Biology Processing Group from January 1, 2003, to December 31, 2006, (NASA OBPG, 2020). These variables were obtained at a spatial resolution of 1 km except for temperature which has a resolution of 4 km. NPP was generated from the Carbon, Absorption, and Fluorescence Euphotic resolving (CAFE) NPP model (Behrenfeld et al., 2005; Silsbe et al., 2016). In this model, NPP is calculated by multiplying the energy absorption ($Q_{PAR}$) and efficiency of converting absorbed energy into carbon biomass($\phi_u$). The efficiency is defined as the maximum efficiency multiplied by the decrease in photosynthetic efficiency as incident light increases.

To serve as inputs in the NEMURO-GOM model equations, the total phytoplankton carbon biomass must be partitioned into small and large phytoplankton biomass. This partitioning uses absorption and scattering coefficients that vary with phytoplankton size to retrieve pico- and microphytoplankton percentages (Mouw & Yoder, 2010). The resulting daily size fractionation fields were multiplied by the total phytoplankton carbon biomass to obtain large and small phytoplankton biomass. Due to significant cloud cover, ocean color data in the GoM is limited (Figure 1), with spatial variations ranging from 3 to 35% cloud free pixels from 2003 through 2006.

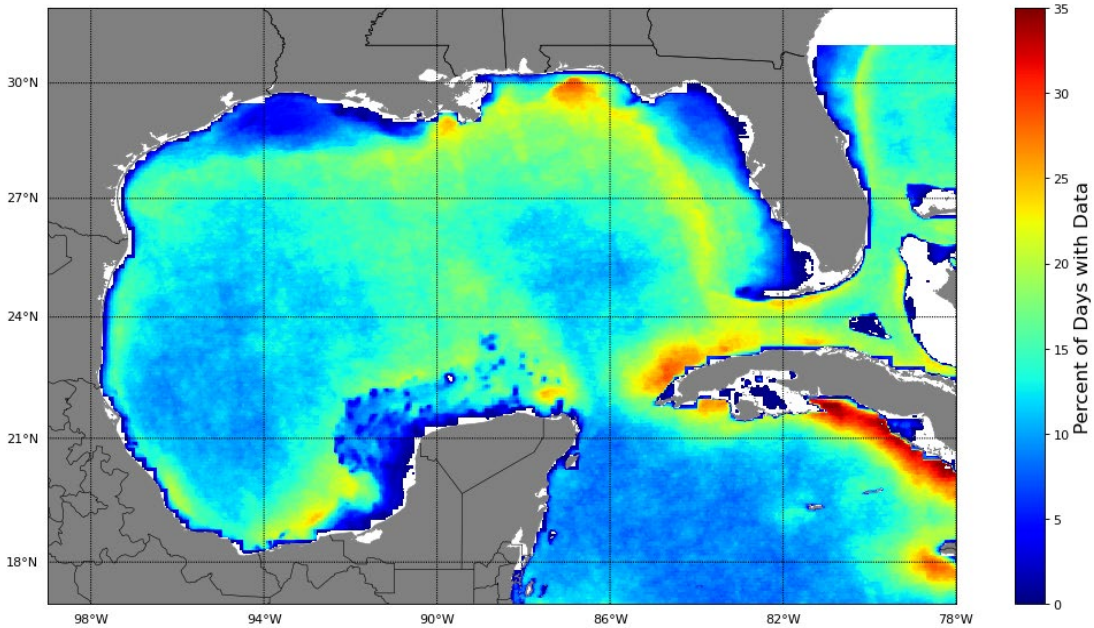


Figure 1: The percentage of days with remote sensing data from the MODIS Aqua sensors in the Gulf of Mexico from January 1, 2003, to December 31, 2006.

**Eddy tracking algorithm and validation**

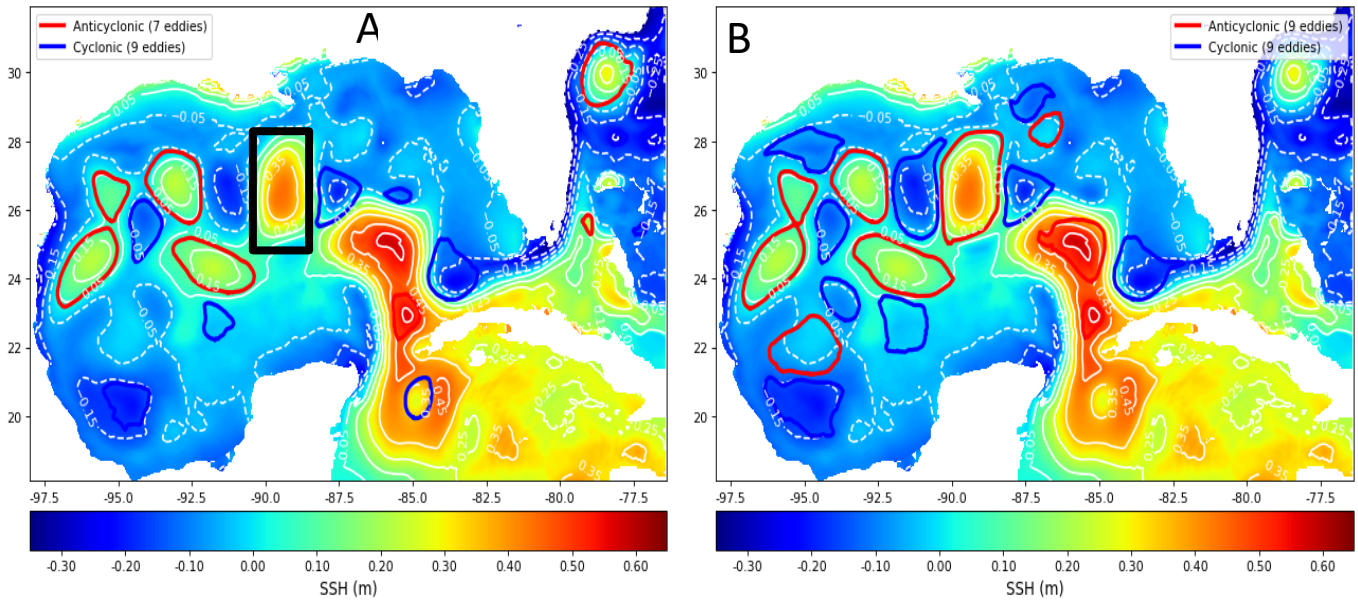


Figure 2: Changes in eddy detection when setting maximum number of local extrema in contour to 1 (A) and setting maximum number of local extrema in contour to 4 (B). Black rectangle represents a previously undetected anticyclonic eddy.

To detect and identify eddies in the Gulf of Mexico, we used Py-Eddy-Tracker (Chelton et al., 2011; Mason et al., 2014, 2017). This software uses SSH as input which we obtained from HYCOM-GoM with a spatial resolution of 4 km. The algorithm separates features into cyclonic and anticyclonic eddies based on negative or positive sea level anomaly, respectively. Eddies are detected as closed SSH contours with the outermost edge of the eddy referred to as the effective contour. The algorithm also detects a maximum circum-averaged speed contour within each eddy. In addition to the effective and speed contours, the algorithm outputs a variable which represents the number of equally spaced SSH contours contained within that eddy. Putative eddies may be rejected based on criteria such as eddy shape error, pixel count, an amplitude threshold, or the number of local SLA maxima for anticyclones and SLA minima for cyclones. A

sensitivity analysis (See Supplemental Information) was conducted by individually varying the criteria used to detect eddies to determine their effect on eddy detection. The shape error was slightly adjusted from 55% to 60%. The maximum SSH pixel limit was changed to 20000 to ensure that larger eddies, such as loop current eddies were detected. Adjustment of the maximum number of local extrema (MNLE) within a contour had the greatest impact on eddy detection. Figure 2 contrasts the MNLE parameter that varies from 1 (Figure 2A) to 4 (Figure 2B) The black rectangle on Figure 2A surrounds an anticyclonic eddy which is not detected until the MNLE reaches 4. The adjusted algorithm also detects a suspected cyclonic eddy at 92°W and 26°N that went previously undetected. Furthermore, eddies outside of the GoM basin which were previously detected are no longer included. After investigating each parameter in isolation, the revised values were combined to create the new algorithm which better represents the physical dynamics of eddies in the Gulf of Mexico.

To further validate the improvements in the adjusted algorithm, visual analysis determined the changes in false positives and false negatives between the original algorithm and the adjusted algorithm. Two equally spaced days per month were visually evaluated to count the number of false positives and negatives from each algorithm version. False positives were defined as eddies the algorithm detected but did not display the usual characteristics of an eddy and false negatives were eddies that exhibited the characteristics of an eddy but were not detected by the algorithm. The number of anticyclonic false positives were reduced by 55% from 124 to 56 and the number of anticyclonic false negatives were reduced by 70% from 148 to 44 using the new parameter set. The number of cyclonic false positives was reduced by 34% from 128 to 84 and the number of cyclonic false negatives was reduced by 58% from 172 to 72 with the revised parameters. The greatest improvement in the algorithm results from detecting more

anticyclonic eddies which is ideal as we want to capture the Loop Current eddies propagating westward across the oligotrophic GoM (Vukovich, 2007).

**Eddy detection and implementation**

HYCOM-GoM SSH was masked to remove the Gulf Stream on the east coast of Florida and Georgia to focus solely on eddies within the Gulf of Mexico basin. Because the eddy and satellite fields have different spatial resolutions, the satellite data was regridded using the Earth System Modeling Framework Universal Regridder for Geospatial Data package in python (xESMF). The regrid method chosen was bilinear interpolation which interpolates the data using recurrent linear interpolation which does not create new maximum and minimum data points and is recommended on rectangular grids (Jiawei et al., 2023). The eddy fields and satellite fields were then combined to investigate the impact of anticyclonic and cyclonic eddies directly on fields such as small phytoplankton biomass, large phytoplankton biomass, and NPP for small and large phytoplankton as well as the satellite-derived estimates of small, large, and predatory zooplankton and the grazing associated with each zooplankton size class. The following values were obtained:

1. Eddy Centers: The value of all variables within anticyclonic and cyclonic eddies were obtained by masking data outside the 4$^{th}$ equally spaced contour from the central point of an eddy and then calculating the median of the retained pixels.
2. Eddy Edges: Edge data was computed by taking the median of data around the maximum speed contour. This area was defined as the space between contours at 1.1 times the speed contour radius and .9 times the speed contour radius. If 1.1 times the speed contour radius extends outside the eddy boundary, then the outer eddy boundary contour is used instead.

3. Eddy Surroundings: To determine the eddy anomalies relative to the near field data, the median values surrounding the eddies were obtained by masking within each individual eddy boundary and outside a built contour equivalent to 1.5 times the radius of that eddy. This provided a local comparison rather than a basin-wide average that might exclude regional background variability within the basin.

**Statistical analysis and techniques**

To investigate the impacts of eddies on phytoplankton and zooplankton biomass, the differences between median values were calculated using nonparametric tests (center – surrounding, center – edge, edge – surrounding) which provided eddy anomalies for both centers and edges and the differences between the two eddy regions. The Mann-Whitney U Test was used to calculate statistical significance between the eddy distribution. The Kolmogorov-Smirnov test and Anderson Darling test showed that the eddy data is not normally distributed. Therefore, the Mann-Whitney U hypothesis test was used which assumes a non-normally distributed data set compared to a two sample T-test which compares the means of two normally distributed datasets and could skew results.

*Results*

**Spatial and temporal patterns in zooplankton and phytoplankton biomass**

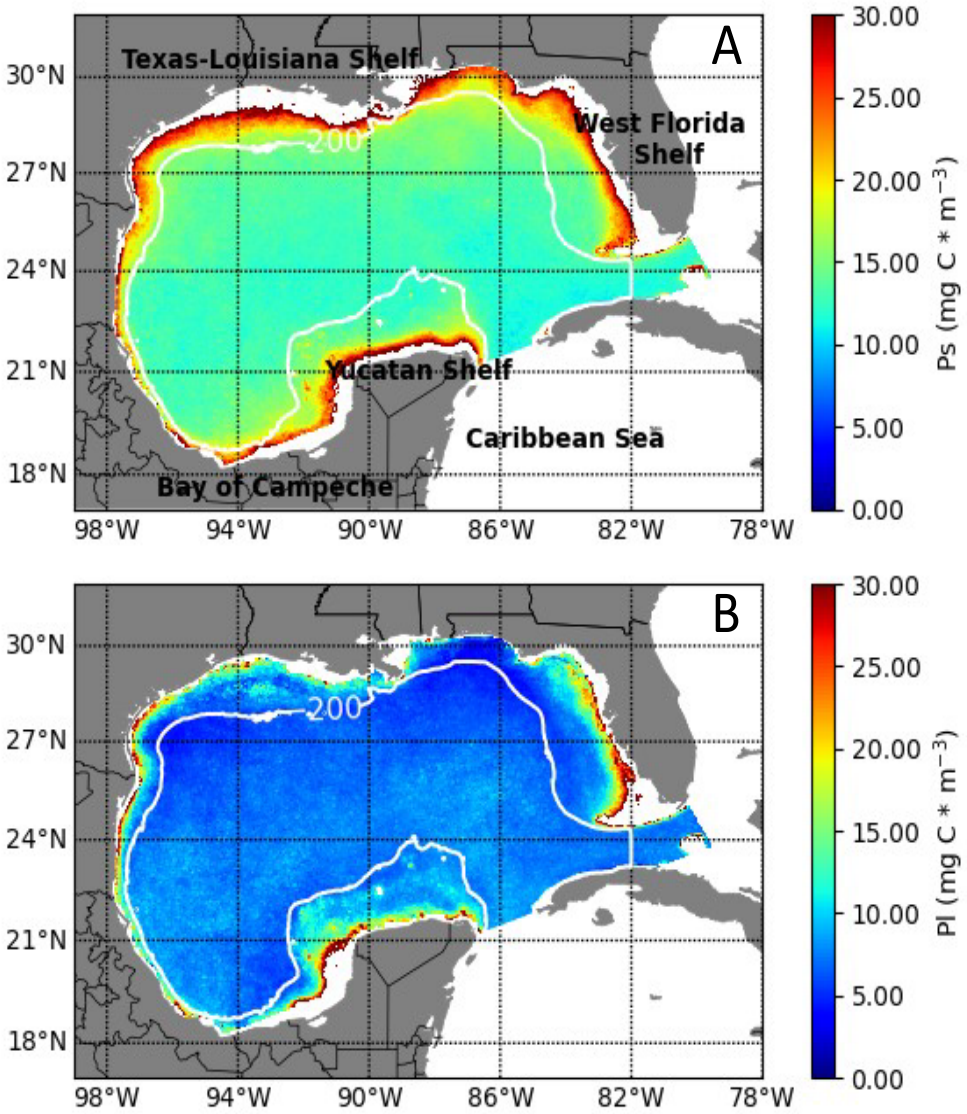

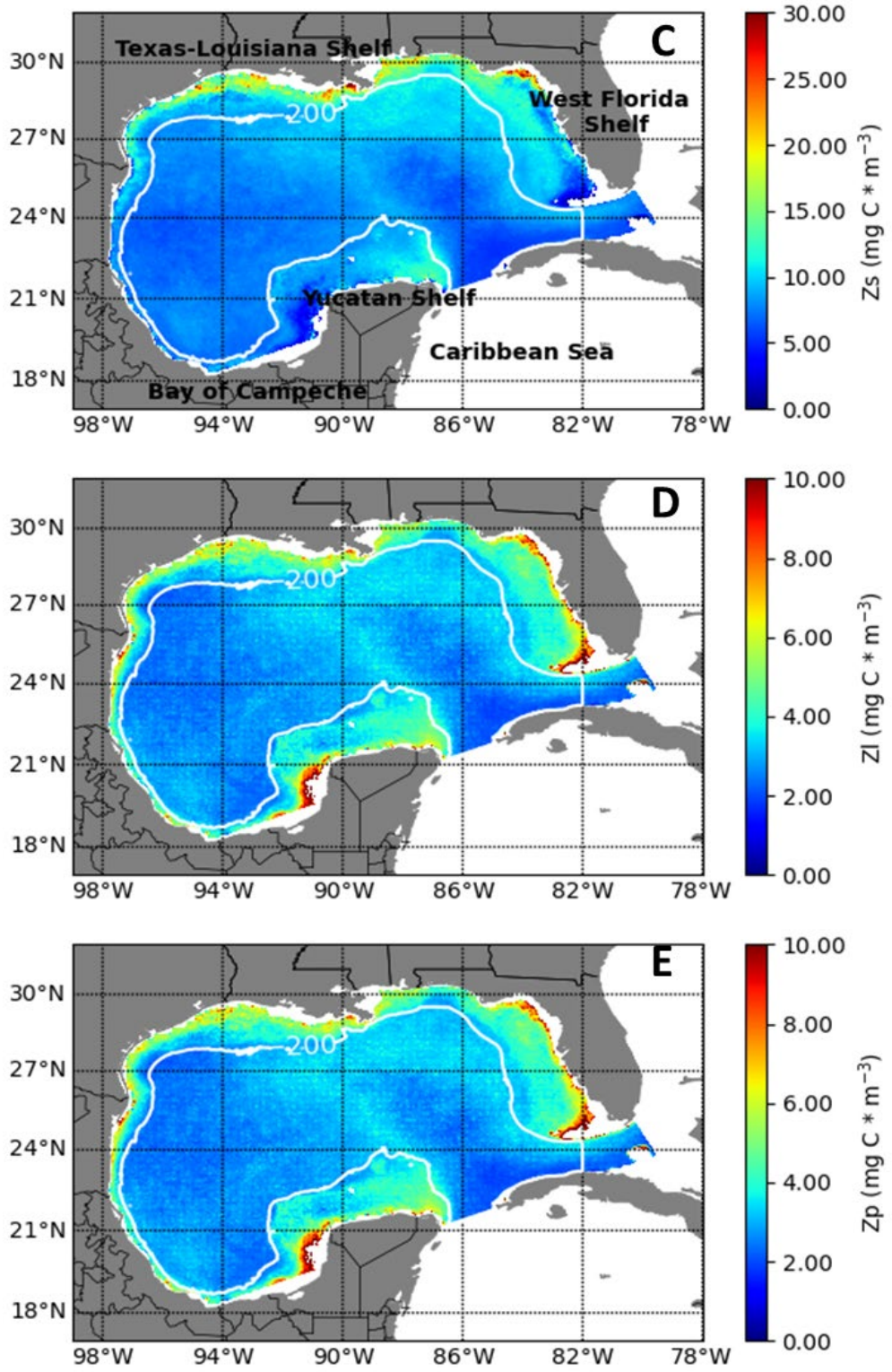


Figure 3: Temporally averaged phytoplankton and zooplankton biomass throughout the GoM for A: Small Phytoplankton B: Large Phytoplankton C: Small Zooplankton D: Large Zooplankton E: Predatory Zooplankton

Average zooplankton and phytoplankton biomasses vary spatially throughout the GoM (Figure 3A-E). Along the continental shelf, increases in biomass in both phytoplankton size classes (Figure 3A-3B) occur along the West Florida Shelf. The inner West Florida Shelf presents higher biomass compared to the outer West Florida Shelf (similar to patterns found in Salmerón-García et al., 2011). These differences may be caused by increased river discharge along the inner West Florida Shelf (Morey et al., 2009) and local wind forcing (Weisberg et al., 2001). In the eastern Gulf of Mexico, the Loop Current and mesoscale eddies can also influence the continental shelf leading to increased coastal upwelling (Muller-Karger, 2000; Weisberg & Liu, 2017). Similarly, the Yucatan Shelf has a large area of elevated biomass closer to the Bay of Campeche than the Yucatan Channel, especially for large phytoplankton which was also found by Salmerón-García et al., 2011. Small phytoplankton have the highest biomass on continental shelves with values averaging 21.45 $mgC/m^3$. However, the variation in biomass across each shelf differ regionally reflecting the different dynamics along each shelf controlling phytoplankton biomass. Previous studies have noted this complexity along the continental shelf and many different regions with varying biogeochemical interactions have been identified (Callejas-Jimenez et al., 2012; Martínez-López & Zavala-Hidalgo, 2009; Muller-Karger et al., 2015). Large phytoplankton show elevated biomass on the shelf, but their abundance is lower on the Texas Louisiana Shelf relative to other shelf biomass hotspots. Large phytoplankton averages biomass values of 11.4 $mgC/m^3$ along the continental shelf. Within the oligotrophic abyssal plain between 24°N and 27°N, there are patchy increases in biomass, especially evident in the large phytoplankton. Small phytoplankton average biomass within the oligotrophic GoM is 12.6 $mgC/m^3$. Small phytoplankton accounts for approximately 77.5% of total phytoplankton biomass

in the open ocean GoM while large phytoplankton accounts for approximately 22.5%. This is consistent with Gomez et al., 2018 which found that nanophytoplankton (small phytoplankton) made up 80% or more of the total phytoplankton in the oceanic region of the GoM.

Zooplankton (Figure 3C-E) also have elevated biomass along the shelf but the spatial patterns differ from phytoplankton. Small zooplankton shows significantly lower biomass along the inner West Florida Shelf compared to the outer West Florida Shelf. This pattern is also evident in large and predatory zooplankton but with weaker gradients. Small zooplankton show elevated biomass along the inner Texas-Louisiana shelf, echoing the maxima in phytoplankton biomass, but do not have elevated biomass inshore along the Yucatan Shelf, or around the western perimeter of the GOM, as on the West Florida Shelf. This may be due to grazing pressure by larger zooplankton groups. Regionally, we see that the western GoM basin typically has lower zooplankton biomass across all three size classes compared to the northeastern GoM basin. Also, the Loop Current region has low biomass in all three zooplankton size classes. All three size classes of zooplankton biomass do not differ greatly between the average shelf biomass and average open ocean GoM biomass. Average small zooplankton along the shelf and within the open ocean GoM is 7.7 $mgC/m^3$ and 7 $mgC/m^3$, respectively. Average large zooplankton along the shelf and within the open ocean GoM is 6.3 $mgC/m^3$ and 4.2 $mgC/m^3$, respectively. Average predatory zooplankton along the shelf and within the open ocean GoM is 6.1 $mgC/m^3$ and 3.9 $mgC/m^3$, respectively. These differences are much smaller than the doubling observed for phytoplankton. Small zooplankton account for approximately 27% of total zooplankton biomass in the open ocean GoM while large and predatory zooplankton account for

approximately 39% and 34%, respectively. The Campeche Bank region has consistently elevated biomass for all zooplankton size classes, but particularly for large and predatory sizes.

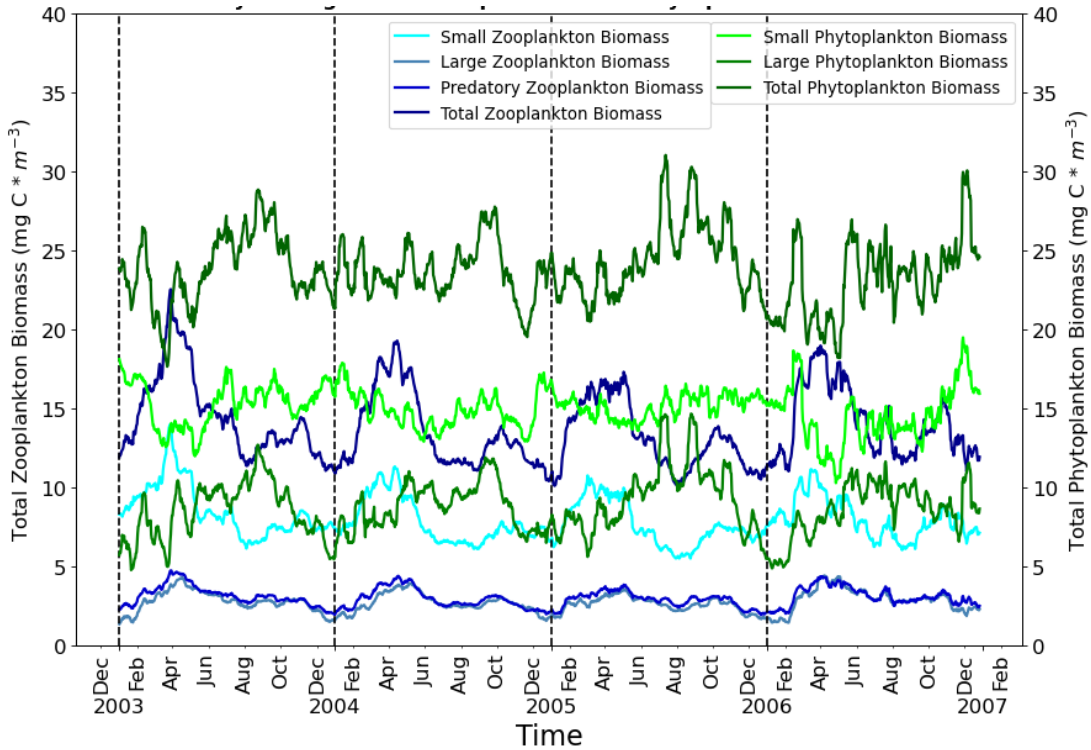


Figure 4: Daily averaged total surface zooplankton and phytoplankton biomass in the Gulf of Mexico

Total phytoplankton biomass is higher than the zooplankton biomass in late summer and early fall while total zooplankton biomass is higher than total phytoplankton biomass in the spring (Figure 4). Small phytoplankton biomass is the highest biomass of the 5 size classes of plankton and shows little seasonal variability. Conversely, the large phytoplankton variability dominates the seasonality in total phytoplankton biomass. The 3 size classes of zooplankton all contribute to the seasonality of the total zooplankton biomass, but small zooplankton biomass is dominant. Small zooplankton has the highest biomass while large and predatory zooplankton have similar seasonality. Small zooplankton has the lowest biomass of all 5 size classes of plankton biomass. The average total zooplankton biomass from 2003 through 2006 is 16.1 mgC/m$^3$, 19.6 mgC/m$^3$, 14.5 mgC/m$^3$, and 14.1 mgC/m$^3$ for winter, spring, summer, and fall,

respectively. For total phytoplankton biomass, the seasonal average is 22.9 mgC/m$^3$, 22.8 mgC/m$^3$, 24.6 mgC/m$^3$, and 24.5 mgC/m$^3$ for winter, spring, summer, and fall, respectively.

**General patterns in cyclonic and anticyclonic eddies**

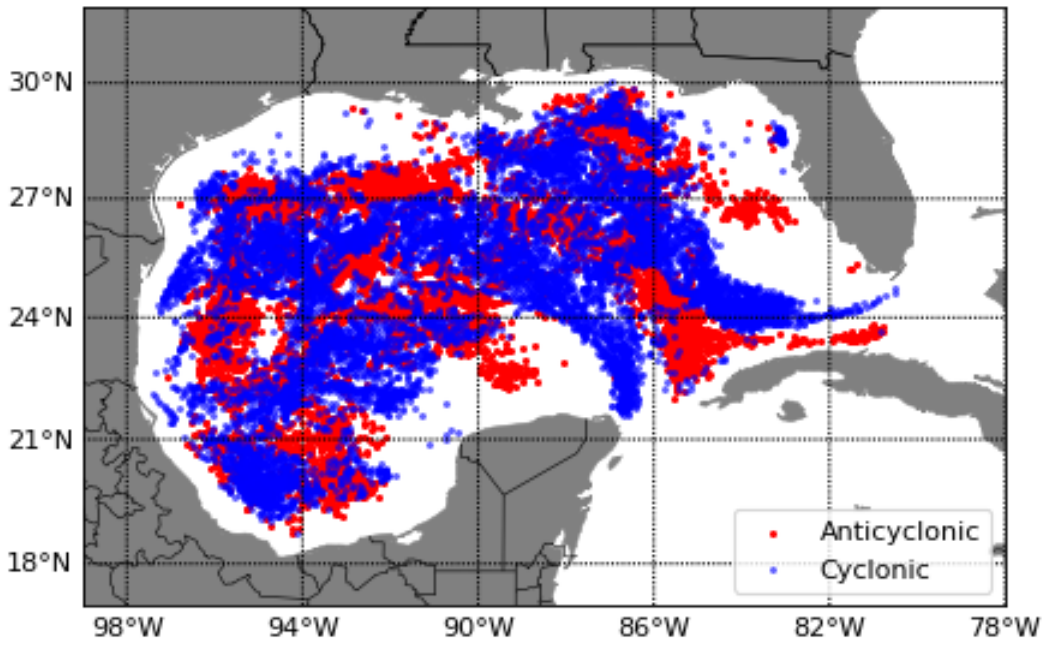


Figure 5: Geographical location of the center longitude and latitude for all cyclonic and anticyclonic eddies from 2003 through 2006 in the Gulf of Mexico

The eddy algorithm detected 11,240 cyclonic eddies and 9,698 anticyclonic eddies in 1,496 daily images from 2003 to 2006. The eddy locations are shown in Figure 5. It is important to note that these are not different eddies, but snapshots of eddy position and characteristics daily. Hence, there are patterns in eddy detection locations that emerge due to the propagation of both anticyclonic and cyclonic eddies across the GoM. During this period, daily snapshots of 5,918 anticyclonic eddies and 5,966 cyclonic eddies occurred in the western region of the GoM (delineated by the 89.96°W meridian following Muller-Karger et al., 2015) which is 61% and 53% of the total number of eddies detected in the whole basin, respectively. The abyssal plain

and continental slope make up 65% of the total Gulf of Mexico area. Most eddies occur over the abyssal plain and approximately 18% and 14.2% of the non-shelf GoM is occupied by an anticyclonic or cyclonic eddy on average. This indicates that eddies play an important role in setting the characteristics of the basin at large. Mean amplitude, expressed as the magnitude of the difference between the extremum of SSH within the eddy and the SSH around the contour representing the outermost eddy boundary, is .1 and .09 meters in the western GoM for anticyclonic and cyclonic eddies. In contrast, the eastern GoM has a mean amplitude of .15 and .14 meters for anticyclonic and cyclonic eddies corresponding to 33% and 36% increases in eastern GoM mean amplitude. As expected, the average maximum eddy speed is also higher in the eastern GoM for both anticyclonic and cyclonic eddies with speeds of .4 m/s and .37 m/s in the western GoM and .63 and .61 m/s in the eastern GoM. The elevated speed and amplitude in the eastern GoM could be a result of eddies that have just shed from the Loop Current and have not yet propagated westward.

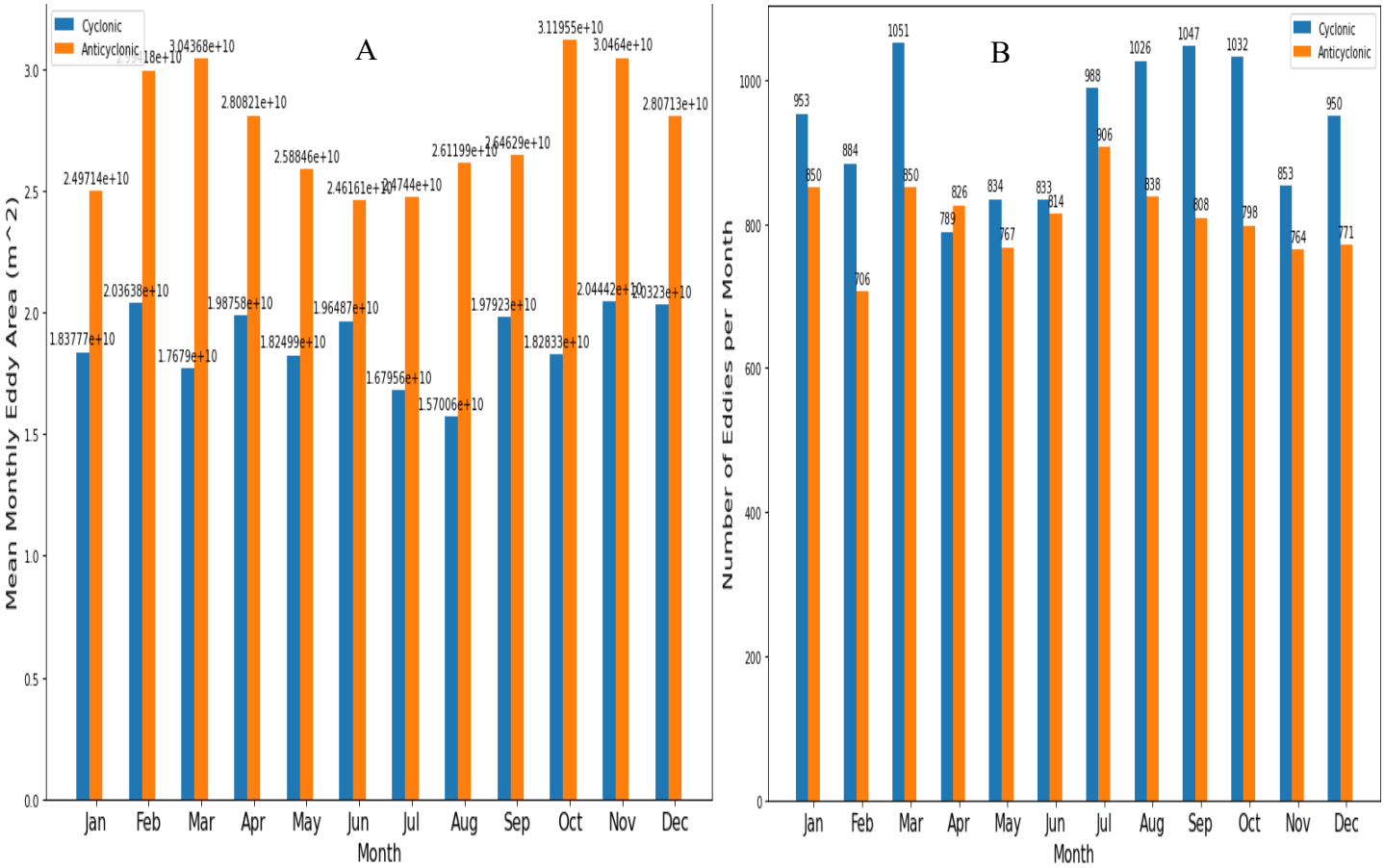


Figure 6: Mean monthly eddy area (A) and number of eddies (B) for cyclonic and anticyclonic eddies per month in the Gulf of Mexico

GoM eddy frequency differs across the seasons (Figure 6B). Cyclonic eddies show a bimodal distribution, having two peaks, one in late Winter and one in late Summer/early Fall while the number of anticyclonic eddies is more uniform throughout the seasons which is consistent with the findings of (Zhu & Liang, 2022). In almost every month, there are more cyclonic eddies than anticyclonic eddies, though in April through June, the numbers are similar. Because the sizes of the anticyclonic and cyclonic eddies differ on average, the areal extent of the GOM that falls within an eddy varies over time differently than the eddy number (Figure 6A). Anticyclonic eddies have larger sizes than the cyclonic eddies however, which amplifies

their importance in areal extent compared to number of eddies. Figure 6A illustrates this pattern, with anticyclonic eddy integrated area greater across all months than cyclonic eddy integrated area. Interestingly, the Spring minimum in eddy count for cyclonic eddies is not mirrored in the areal extent, suggesting that cyclonic eddies in Spring tend to be larger. The anticyclonic areal extent has a bimodal distribution peaking in Spring and Fall, driven by eddy size rather than eddy number. Cyclonic eddy area is consistent throughout the year. Seasonally, the percentage of the abyssal plain occupied by a cyclonic eddy is 14.9%, 13.3%, 13.2% and 15.4% for Winter, Spring, Summer, and Fall, respectively. For anticyclonic eddies, the percent areal coverage is 17.5%, 18.5%, 17.3% and 18.8%, respectively.

**Impact of cyclonic and anticyclonic eddies on the planktonic ecosystem**

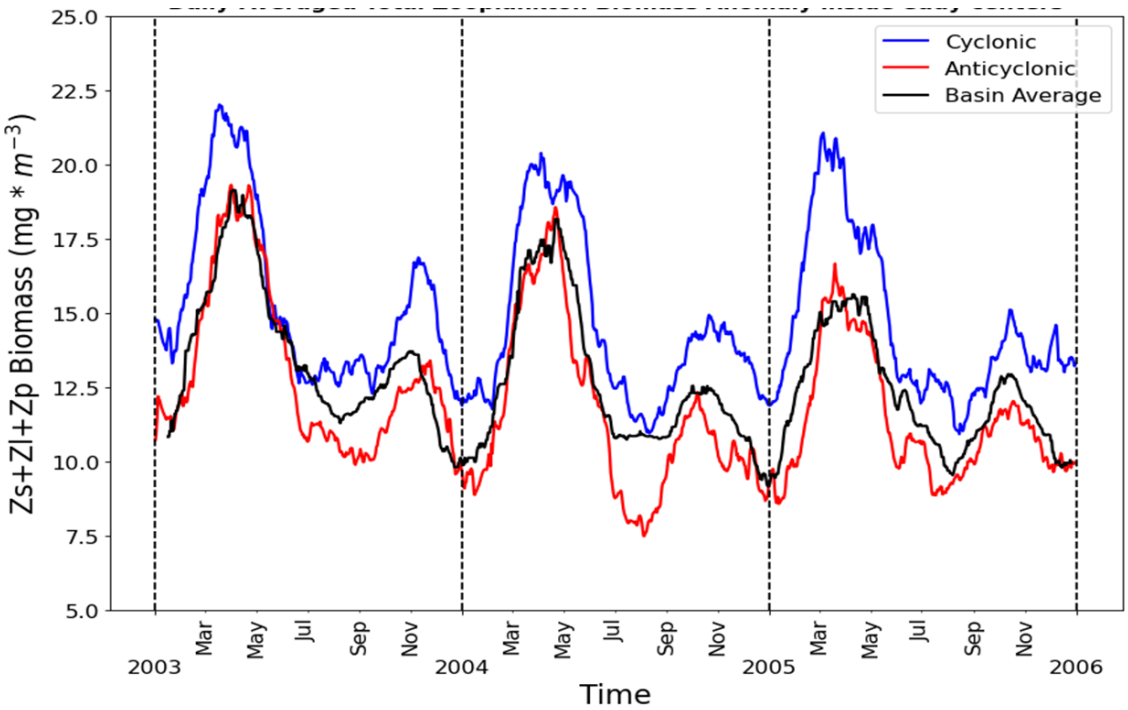


Figure 7: Total daily averaged zooplankton biomass within eddy centers for anticyclonic (red) and cyclonic (blue) eddies and a basin average (black)

Differences in physical dynamics between cyclonic and anticyclonic eddies are expected to lead to variations in the biology and primary and secondary production within eddies (McGillicuddy, 2016). Commensurate with an increase or decrease in phytoplankton biomass, the zooplankton biomass and trophic position might be expected to change (Ryther, 1969). Here, the median aggregated properties in the center of the eddies are presented over the entire period (Figure 7). The seasonal patterns in eddy center biomass are similar to the basin averaged seasonality (Figure 4).

Cyclonic eddy centers have higher total zooplankton biomass compared to the basin average which is greater than the zooplankton biomass in anticyclonic eddy centers. Lower zooplankton biomass in anticyclonic eddy centers is expected due to downwelling within anticyclonic eddy centers. The cyclonic eddies average 17.7 mgC/m$^3$ zooplankton biomass,

compared with 14.3 mgC/m$^3$ anticyclonic biomass and 14.6 mgC/m$^3$ biomass in the GoM across the entire time series. The differences between anticyclonic and cyclonic eddy centers also vary seasonally. For both eddy types, biomass tends to be highest in late winter and early spring and lowest in late Summer and early fall. From February to April, the percent difference between the basin average and eddies is small, -2.4% for anticyclonic eddy centers but the difference increases from July to September to -4.5% for anticyclonic eddy centers, possibly indicating minimal effect of downwelling in winter and much stronger effect of downwelling in summer. For cyclonic eddies, the reverse is true, with enhanced winter impact of upwelling relative to basin average (19.2%) for cyclonic eddy center and reduced upwelling impact in summer (4.7%) for cyclonic eddy center. This implies that cyclonic eddy centers impact zooplankton biomass in the GoM more than anticyclonic eddy centers in late winter and spring while anticyclonic eddy centers impact zooplankton biomass in the GoM more than cyclonic eddy centers in the summer and early fall. Single large and intense eddies that dominate changes in productivity contribute to patchiness in both cyclonic and anticyclonic eddy centers zooplankton biomass.

Figure 7 highlights the difference between anticyclonic and cyclonic eddy centers for zooplankton, but we also want to know how the eddy center biomass compares to the local biomass surrounding each eddy for all trophic levels. Figure 8 displays the median eddy center biomass anomaly for each trophic level and highlights the differences between anticyclonic eddy centers, cyclonic eddy centers, and their respective surroundings. For all trophic levels, cyclonic eddy centers biomass is higher than cyclonic eddy surrounding biomass. Conversely, anticyclonic eddy center biomass is lower than anticyclonic eddy surrounding biomass. The anomalies are relatively symmetrical indicating that the downwelling eddies are still able to depress biomass beyond the oligotrophic surroundings. Small phytoplankton has differences

between eddy center and eddy surrounding of .36 mgC/m$^3$ and -.54 mgC/m$^3$ for cyclonic and anticyclonic eddies, respectively. NPP for Ps is symmetric between the anomalies for cyclonic and anticyclonic eddies with differences of .68 mgC/m$^3$ and -.76 mgC/m$^3$. Zs follows a similar pattern to NPP Ps and Ps with differences between eddy center and eddy surrounding of .73 mgC/m$^3$ and -.72 mgC/m$^3$. Pl is the only trophic level where the anomalies between eddy center and surrounding are not significantly different. Zl and Zp are symmetrical between anticyclonic and cyclonic eddy center and surrounding differences. Furthermore, Zl and Zp have the smallest differences except for Pl between cyclonic eddy centers and anticyclonic eddy centers with differences of .23 mgC/m$^3$ and -21 mgC/m$^3$ for large zooplankton and .25 mgC/m$^3$ and -.22 mgC/m$^3$ for predatory zooplankton.

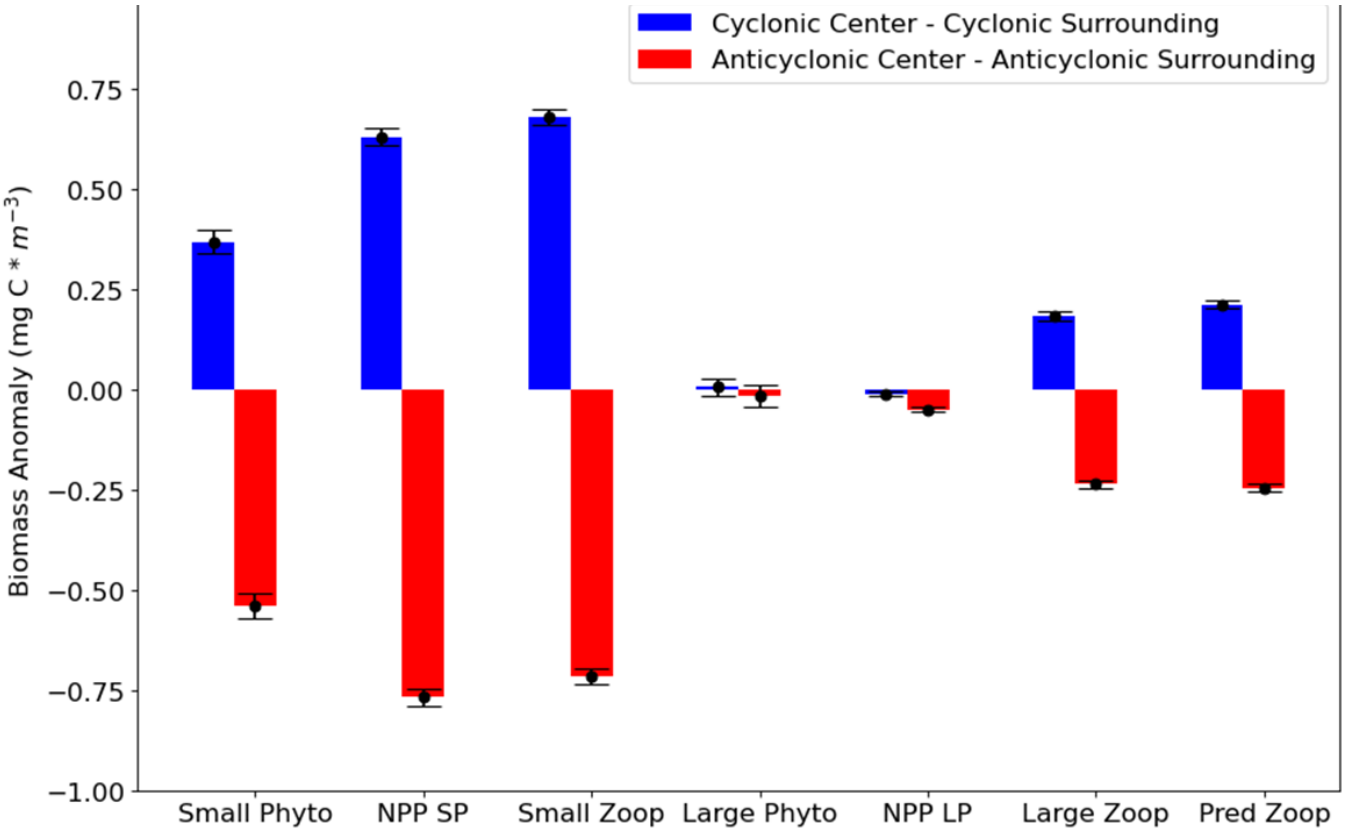


Figure 8: Differences between eddy center and surroundings: cyclonic eddy center and cyclonic eddy surrounding (blue), anticyclonic eddy center and anticyclonic eddy surroundings (red)

**Influence of eddy edge effects on productivity in eddies**

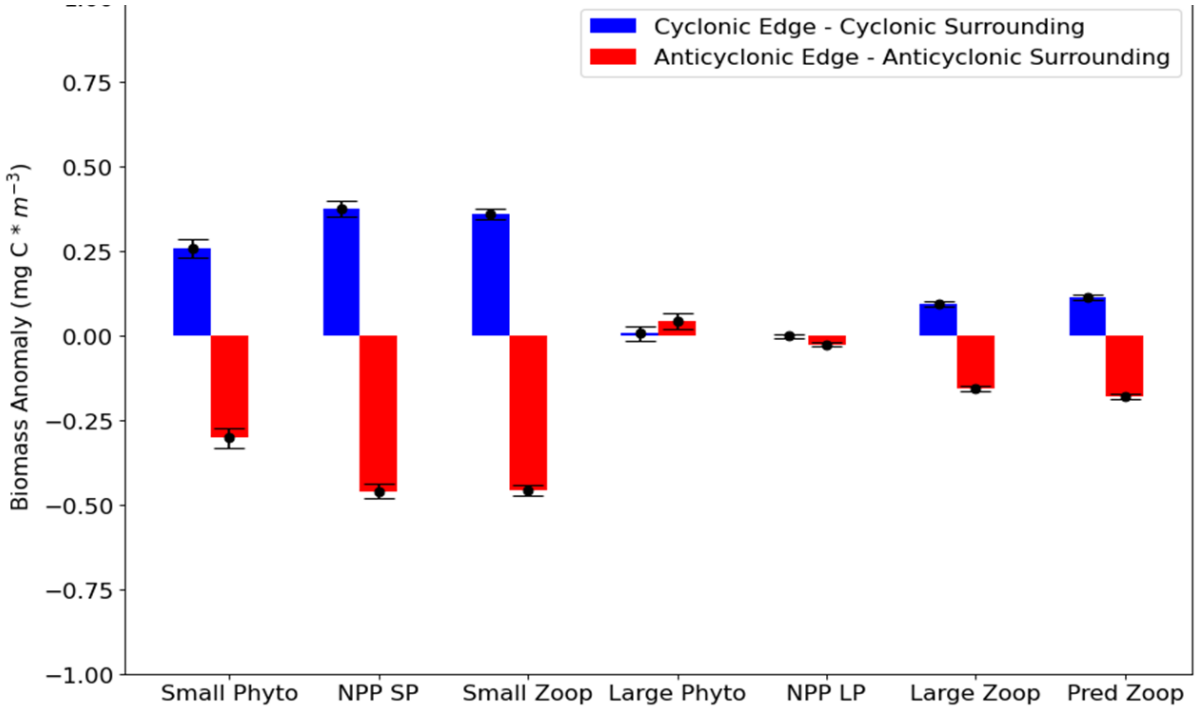


Figure 9: Differences between eddy edges and surroundings: cyclonic eddy edge and cyclonic eddy surrounding (blue), anticyclonic eddy edge and anticyclonic eddy surrounding (red)

To determine how the possibly submesoscale dynamics around the edges of eddies impact ecosystem processes, we compute the biomass through phytoplankton and zooplankton size classes in a band centered on the maximum speed contour associated with the eddy. Figure 9 illustrates the overall effects of eddy edges on plankton biomass and NPP in both cyclonic and anticyclonic eddies compared to eddy surroundings. Like eddy centers, cyclonic eddies have higher biomasses along the edges compared to surroundings. However, the magnitude of the anomaly is less in eddy edges compared to eddy centers. The signal in Pl and NPP Pl is negligent similar to eddy centers. Large and predatory zooplankton along cyclonic eddy edges have an anomaly of .14 mgC/m$^3$ and .16 mgC/m$^3$, respectively. Similarly, large, and predatory zooplankton have anomalies for anticyclonic eddy edges of -.2 mgC/m$^3$ and -.21 mgC/m$^3$,

respectively. Compared to the overall dynamics within eddy centers, the anomalies along edges are less overall.

Overall, eddy edges show differences from the non-eddy surroundings and follow similar patterns to eddy centers. However, there can be variability in the dynamics around the periphery of both anticyclonic and cyclonic eddies where ageostrophic processes leading to vertical motions can result in enhancement or dilution of biomass along eddy edges (Douglass & Richman, 2015; Sánchez-Velasco et al., 2013; Shih et al., 2015; Wang et al., 2018). To better understand how eddies within the GOM differ, we divide them into five groups intended to stratify the eddies based on their indication of submesoscale edge dynamics. These groups are determined by the anomalies in small phytoplankton biomass in the center and edges of the eddies relative to the surroundings of the eddies. This delineation is a bottom-up approach, assuming that the physical dynamics impacts primarily nutrient supply and lowest trophic level small phytoplankton biomass. These eddy groupings are analyzed to understand how physical dynamics interacts with grazing and biomass differences between trophic levels.

The first case consists of eddies that are inconsistent with our understanding of how geostrophic dynamics in eddy centers raise the pycnocline towards the surface (cyclonic) or deepen the pycnocline (anticyclonic). These eddies are identified as cyclonic eddies where the center small phytoplankton biomass is lower than the reference surroundings and anticyclonic eddies with higher center biomass compared to the surroundings.

Cases 2 and 3 delineate eddies where the anticipated effect of geostrophic motions within centers are consistent with small phytoplankton biomass. However, the two cases differ in terms of surface horizontal mixing. In case 2, eddy pumping results in elevated (cyclonic) or diluted (anticyclonic) biomass within centers however this is not translated to the edges which have

higher (lower) biomass than surroundings, but not as high as centers. In case 3, the eddy pumping within centers propagates to the edge possibly through horizontal mixing resulting in similar biomass anomalies between centers and edges. It is important to note that nonlinear vertical motions at the edge could be impacting these eddies, contributing to their biomass distributions, but they cannot be distinguished clearly.

Ageostrophic motions along eddy edges typically act to mix the water column vertically. Depending on the eddy, the process can result in biomass enhancement where the nutricline is raised or the mixing reaches into a deep chlorophyll maximum layer. Vertical mixing can also dilute surface biomass if the vertical motions do not reach into the nutricline (or deep chlorophyll maximum) along the eddy edge. For case 4, instabilities or other processes have resulted in the cyclonic and anticyclonic edge biomasses being higher than the centers and surroundings. From a bottom-up perspective, this suggests vertical motions have lifted the pycnocline enhancing surface biomass. Case 5 includes eddies where the ageostrophic motions have resulted in dilution along the edges due to the vertical mixing stopping before reaching the nutricline. Because the edge biomass behaves differently than both the surrounding and the center biomasses, these two cases could identify eddies with ageostrophic or sub mesoscale instabilities along the edges.

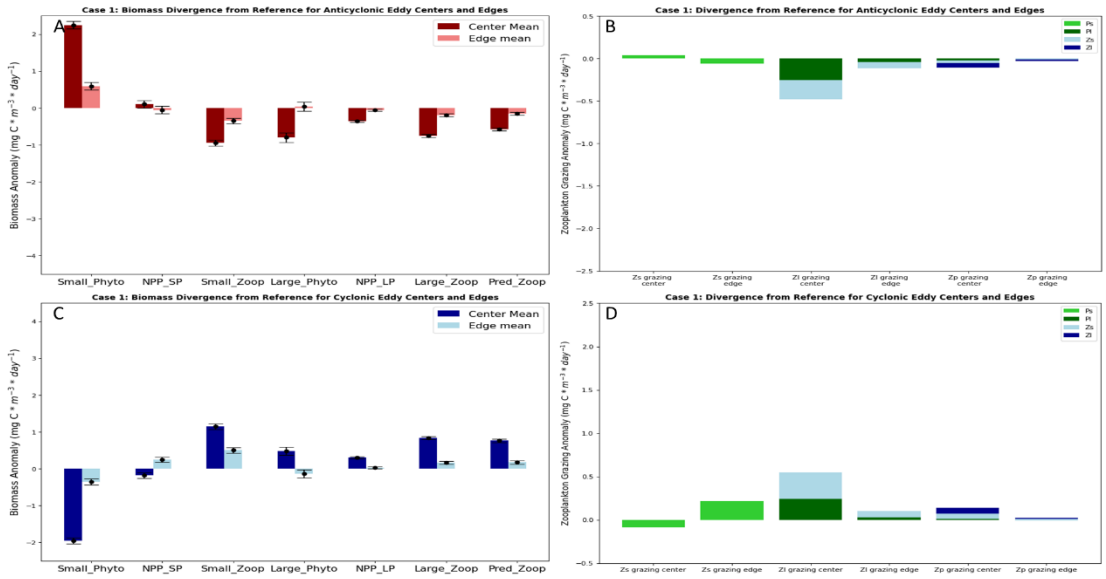


Figure 10: Biomass and grazing anomalies for all plankton size classes and grazing pathways for anticyclonic (A&B) and cyclonic (C&D) eddy centers and edges in case 1

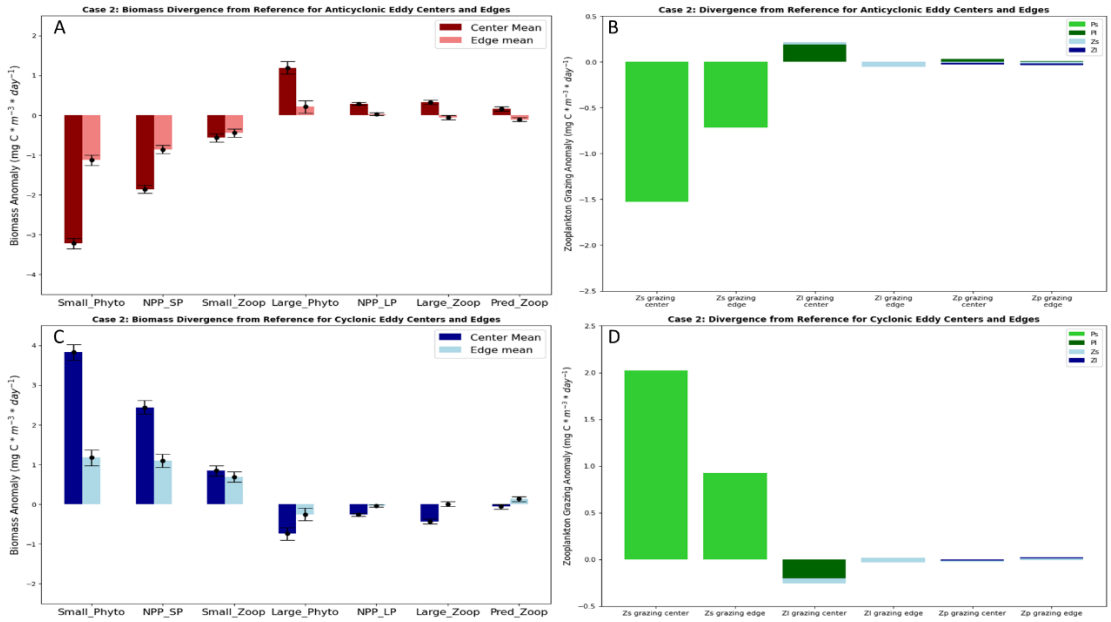


Figure 11: Biomass and grazing anomalies for all plankton size classes and grazing pathways for anticyclonic (A&B) and cyclonic (C&D) eddy centers and edges in case 2

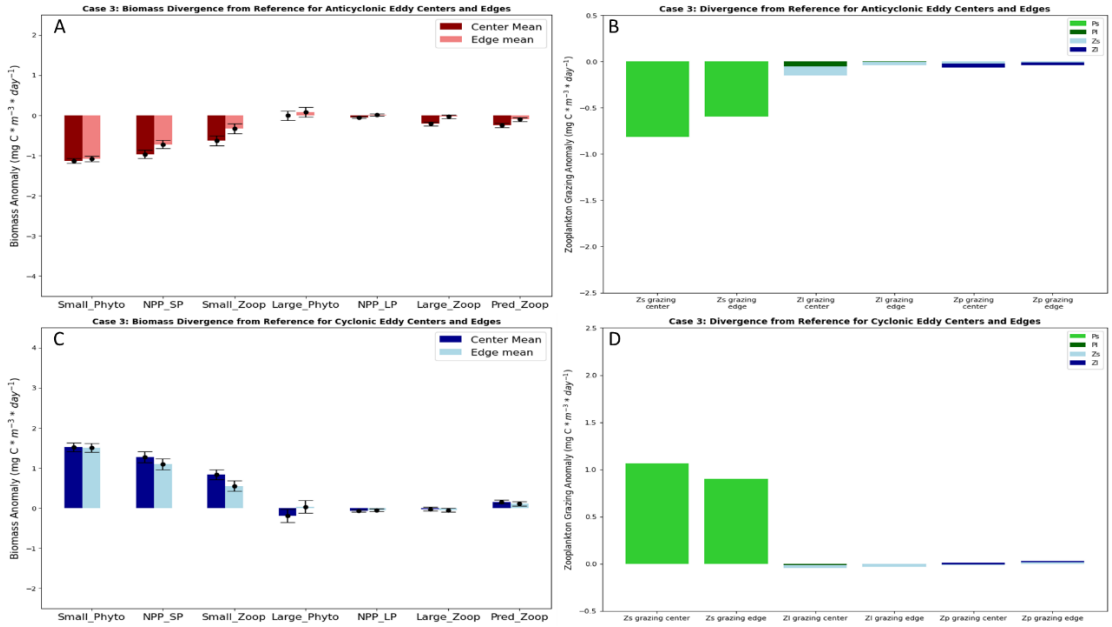


Figure 12: Biomass and grazing anomalies for all plankton size classes and grazing pathways for anticyclonic (A&B) and cyclonic (C&D) eddy centers and edges in case 3

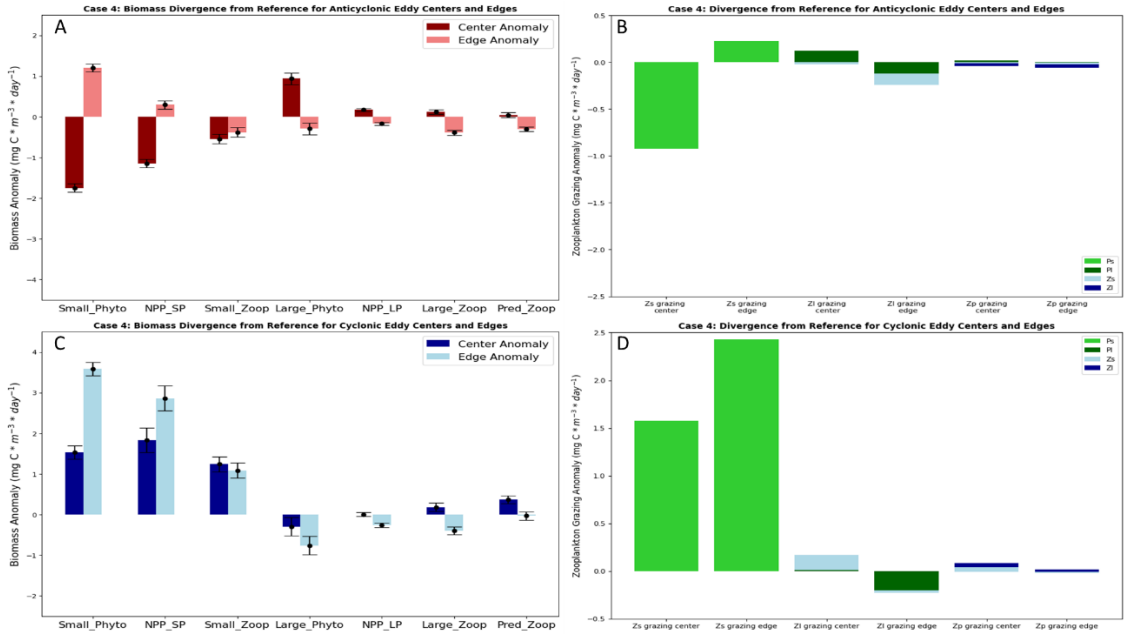


Figure 13: Biomass and grazing anomalies for all plankton size classes and grazing pathways for anticyclonic (A&B) and cyclonic (C&D) eddy centers and edges in case 4

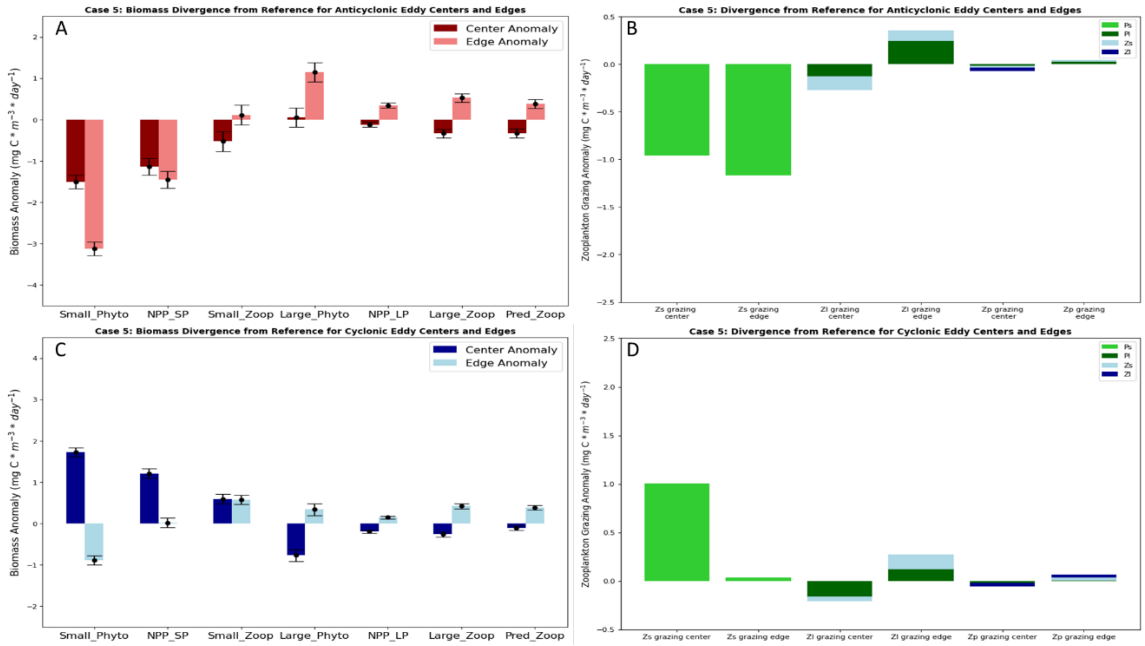


Figure 14: Biomass and grazing anomalies for all plankton size classes and grazing pathways for anticyclonic (A&B) and cyclonic (C&D) eddy centers and edges in case 5

1,332 anticyclonic eddies and 1,601 cyclonic eddies in the GoM have data in all three regions (the edge, center, and surrounding). 550 anticyclonic and 698 cyclonic eddies (41.3% and 43.6 % respectively) are consistent with case 1 (Figure 10) when using small phytoplankton biomass as a measure of response to eddy pumping derived nutrient injection. The average small phytoplankton biomass anomaly for cyclonic eddy centers is -1.95 mgC/m$^3$ and -.35 mg C/m^3 (-14.2% and -2.6% relative to surroundings) for edges. Case 1 eddies have the slowest average cyclonic eddy rotational speed and lowest amplitude of all the cases with mean values of 0.441 m/s and 0.098 m which suggests these eddies are weak and likely older or decaying. While small phytoplankton biomass is inconsistent with our understanding of geostrophic physical impacts on cyclonic eddies, the low biomass does not propagate to higher trophic levels. Case 1 eddies have elevated biomass for large phytoplankton and all three size classes of zooplankton (Figure 10). Case 1 anticyclones have an average small phytoplankton biomass anomaly for eddy centers is 2.25 mgC/m$^3$ and .59 mgC/m$^3$ (17.8% and 4.7% relative to surroundings) for edges. Anticyclones

in case 1 show the opposite pattern from cyclones, with unexpectedly high small phytoplankton biomass, and reduced biomass in large phytoplankton and all zooplankton sizes.

258 anticyclonic and 278 cyclonic eddies fit into case 2 (Figure 11), which is 19.4% and 17.4% of the total, respectively. Case 3 (Figure 12) consists of 215 anticyclonic and 274 cyclonic eddies which are 16.1% and 17.1% of total eddies, respectively. Across the two cases and eddy types, the percentage of eddies within this group is consistent. Case 2 cyclonic eddies (Figure schematic) have an average small phytoplankton biomass anomaly of 3.83 mgC/m$^3$ in centers and 1.17 mgC/m$^3$ in the edge. Case 2 anticyclonic eddies (Figure schematic) have an average small phytoplankton biomass anomaly of -3.22 mgC/m$^3$ in centers and -1.13 mgC/m$^3$ in the edge. Case 3 cyclonic eddies have an average small phytoplankton biomass anomaly of 1.52 mgC/m$^3$ in centers and 1.5 mgC/m$^3$ in the edge. Whereas Case 3 anticyclonic eddies have an average small phytoplankton biomass anomaly of -1.13 mgC/m$^3$ in centers and -1.08 mgC/m$^3$ in the edge. The small phytoplankton biomass anomaly at the center is highest for case 2 cyclonic eddies and lowest for case 2 anticyclonic eddies compared to all the other cases (30.3% and -24% respectively). Cyclonic and anticyclonic eddies in case 2 also have higher speeds than all other cases at .471 m/s and .514 m/s for anticyclonic and cyclonic, respectively. The case 3 average speeds are slower, .439 m/s and .456 m/s for anticyclonic and cyclonic, respectively. For both case 2 and 3, center and edge biomass are consistent through trophic levels to zooplankton. Large phytoplankton are the exception, with small anomalies opposing the predicted response. The differences between center and edge are smaller for the three size classes of zooplankton compared to small phytoplankton, with small zooplankton biomass anomaly displaying similar edge and center anomaly in cyclonic case 2 eddies and a positive center anomaly in anticyclonic case 2 eddies. For case 3 eddies, the patterns shown in small phytoplankton propagate to the

higher trophic levels. The difference between edge and center anomaly are higher in predatory and large zooplankton for both anticyclonic and cyclonic eddies compared to lower trophic levels phytoplankton and small zooplankton.

Case 4 (Figure 13) consists of 223 anticyclonic and 102 cyclonic eddies which is 16.7% and 6.4% of total eddies respectively whereas Case 5 (Figure 14) has 86 anticyclonic and 249 cyclonic eddies which are reversed at 6.5% and 15.5% respectively. This suggests that more cyclonic eddies experience dilution (case 5) along their edges and more anticyclonic eddies experience enhancement (case 4) along their edges. Case 4 cyclonic eddies have an average small phytoplankton biomass anomaly of 1.54 mgC/m$^3$ in centers and 3.58 mgC/m$^3$ in the edge. Case 4 anticyclonic eddies have an average small phytoplankton biomass anomaly of -1.75 mgC/m$^3$ in centers and 1.2 mgC/m$^3$ in the edge. Case 5 cyclonic eddies have an average small phytoplankton biomass anomaly of 1.73 mgC/m$^3$ in centers and -.89 mgC/m$^3$ in the edge. Case 5 anticyclonic eddies have an average small phytoplankton biomass anomaly of -1.51 mgC/m$^3$ in centers and -3.12 mgC/m$^3$ in the edge. The average speed is higher in case 5 for anticyclonic compared to case 4 and higher in case 4 for cyclonic eddies compared to case 5. The average speed for case 4 is .415 m/s and .484 for anticyclonic and cyclonic eddies, respectively. The average speed for case 5 is .44 m/s and .456 for anticyclonic and cyclonic eddies, respectively. Interestingly, case 4 anticyclonic speed is second lowest and similar to case 1 anticyclonic eddies. For case 4 anticyclonic, we see differences between small phytoplankton biomass anomaly and higher trophic levels. In large and predatory zooplankton, the edge biomass is lower than the surrounding even though biomass is higher in the small phytoplankton. For case 4 cyclonic eddies, all trophic levels follow similar patterns except for large phytoplankton. However, the three size classes of zooplankton show slightly higher centers than edges while

small phytoplankton has much higher edge anomaly compared to centers. For case 5 anticyclonic and cyclonic eddies, the small phytoplankton biomass anomaly does not propagate through the trophic levels. Instead of seeing edges less than the surrounding, we see the opposite for case 5 cyclonic zooplankton biomass for all three size classes. In case 5 anticyclonic eddies, the patterns are consistent in anticyclonic eddy centers but not the edges with only small phytoplankton biomass and NPP having negative anomalies.

**Role of zooplankton grazing and trophic transfer in eddies**

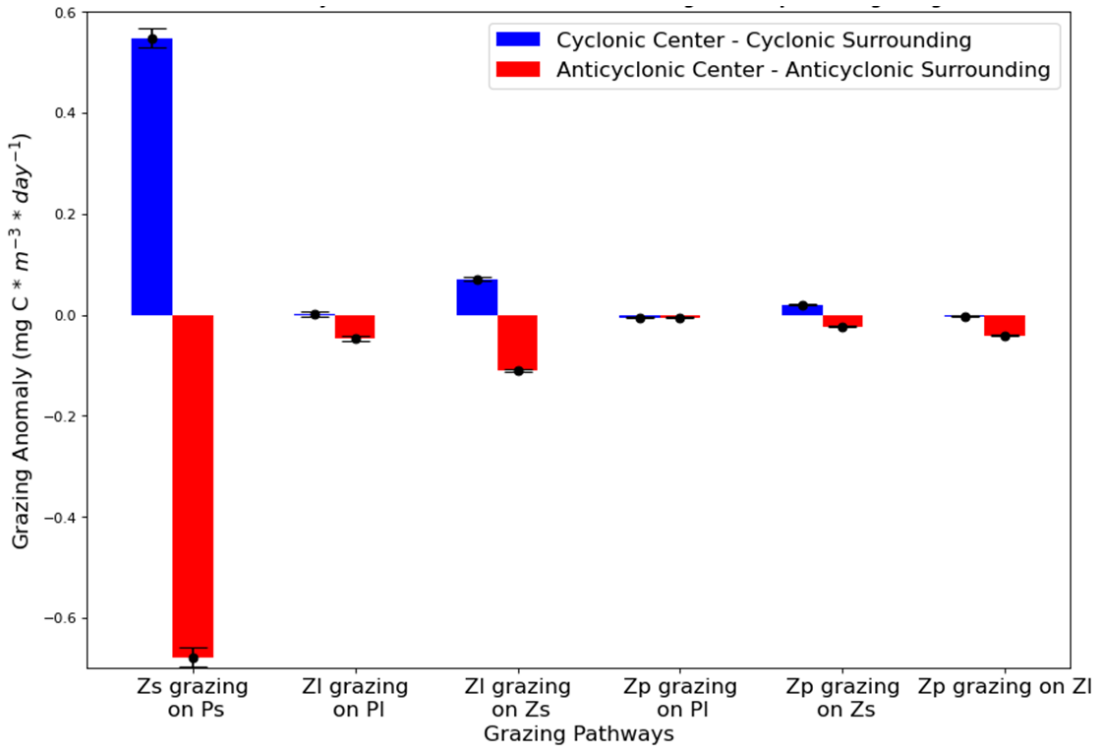


Figure 15: Differences between eddy centers and surroundings for zooplankton grazing: cyclonic eddy center and surrounding (blue), anticyclonic eddy center and surrounding (red)

Zooplankton graze through multiple pathways based on their size in the environment as in our model. In NEMURO-GoM, small zooplankton graze on small phytoplankton. Large zooplankton graze on small phytoplankton and large phytoplankton. Predatory zooplankton graze on large phytoplankton, small zooplankton, and large zooplankton. Figure 15 illustrates the grazing anomaly compared to the surrounding region of the eddy for each zooplankton size class and each grazing pathway within cyclonic and anticyclonic eddy centers. Small zooplankton grazing on small phytoplankton is higher in cyclonic centers by .52 mg C $m^{-3}$ $day^{-1}$. Similarly, the small zooplankton grazing is lower in anticyclonic centers compared to surrounding by -.66 mg $Cm^{-3}$ $day^{-1}$. The anomalies for large zooplankton grazing on large phytoplankton are negligible for cyclonic eddies and .05 mg $Cm^{-3}$ $day^{-1}$. Large zooplankton graze higher on small

zooplankton in cyclonic and anticyclonic eddy centers compared to surroundings by .08 and .11 mg $Cm^{-3}$ $day^{-1}$ respectively. The anomalies are larger for small zooplankton than for large phytoplankton, reflecting the importance of a tight microbial recycling loop.

**Grazing within each eddy case**

Case 1 eddies are those that display inconsistent negative small phytoplankton biomass anomaly for cyclonic eddies and positive biomass anomaly for anticyclonic eddies (Figure 10). Small zooplankton grazing on small phytoplankton follows the same pattern as small phytoplankton biomass with negative biomass anomaly of -.09 mg $Cm^{-3}$ $day^{-1}$ in cyclonic eddy centers and .04 mg $Cm^{-3}$ $day^{-1}$ in anticyclonic eddy centers (-1.4% and .7% relative to surroundings). While the biomass anomalies are symmetric between cyclones and anticyclones, the grazing anomalies are much smaller for the anticyclones suggesting that top-down control of biomass differs between the two cases and is greater for cyclones. As for the biomass in case 1 (Section 3), all other grazing pathways not involving Ps are positive in cyclonic eddy centers and negative in anticyclonic eddy centers consistent with geostrophic nutrient flux increases in cyclones and decreases in anticyclones that lead to faster rates that are decoupled from biomass anomalies. Large zooplankton grazing on large phytoplankton is higher than the surroundings in cyclonic eddy centers (.25 mg $Cm^{-3}$ $day^{-1}$ and 29.6%) and lower than the surroundings in anticyclonic eddy centers (-.26 mg $Cm^{-3}$ $day^{-1}$ and -30.8%). Large zooplankton graze on small zooplankton (.3 mg $Cm^{-3}$ $day^{-1}$ and 40.6%) more than for surroundings in cyclonic eddy centers but have similar reductions in grazing for both large phytoplankton and small zooplankton (-.23 mg $Cm^{-3}$ $day^{-1}$ and 31.9%) in anticyclonic eddy centers. Predatory zooplankton grazing on large phytoplankton is not significantly different than surroundings in either eddy centers or edges, however predatory zooplankton grazing on small and large zooplankton are higher in cyclonic

eddy centers compared to surroundings (.06 mg $Cm^{-3}$ $day^{-1}$ and 42.9% and .07 mg $Cm^{-3}$ $day^{-1}$ and 33.5%). Conversely, predatory zooplankton grazing on small and large zooplankton are lower in anticyclonic eddy centers compared to surroundings (-.03 mg $Cm^{-3}$ $day^{-1}$ and -27.1% and -.06 mg $Cm^{-3}$ $day^{-1}$ and -28.8%). Grazing which occurs at eddy edges in case 1 displays similar patterns to the biomass with reduced intensity of signal at edges compared with centers. Along the edges, small zooplankton grazing on small phytoplankton in cyclonic and anticyclonic eddies is .22 and -.15 mg $Cm^{-3}$ $day^{-1}$ which is 3.6% and 1.2% relative to the surroundings. See Table 1 for values.

Case 2 eddies have elevated or depressed central small phytoplankton biomass, but this anomaly is smaller in the edges (Figure 11). Zs grazing on Ps matches the Ps biomass anomalies (2 mg $Cm^{-3}$ $day^{-1}$ and 36.5%) in cyclonic eddy centers and in anticyclonic eddy centers (-1.5 mg $Cm^{-3}$ $day^{-1}$ and -26.9%) relative to surroundings. Zl grazing on Pl is not very different from the surroundings in either edge of cyclonic and anticyclonic eddies, however the Zl grazing on Pl is 22.4% higher than the surroundings in cyclonic eddy centers with a value of -.2 and 23.1% lower than the surroundings in anticyclonic eddy centers with a value of .19 mg $Cm^{-3}$ $day^{-1}$. Zp grazing on Zs and Zl are 17.1% higher and 8% lower in anticyclonic eddy centers compared to surroundings. Along the edges, Zs grazing on Ps in cyclonic and anticyclonic eddies is elevated and depressed, consistent with biomass anomalies, but smaller in magnitude than the center differences (.93 mg $Cm^{-3}$ $day^{-1}$, 16.7% and -.72 mg $Cm^{-3}$ $day^{-1}$, -12.8%). Zp grazing on Zs has the highest change in cyclonic edges with an increase of 16.5% and Zp grazing on Zs has the highest change in anticyclonic edges relative to the surroundings. See Table 1 for values.

Case 3 eddies are consistent with geostrophic motion but with no difference between center and edge, and with overall much smaller anomalies than case 2 (Figure 12). Zs grazing on

Ps has an anomaly of 1.06 mg $Cm^{-3}$ $day^{-1}$ in cyclonic eddy centers and -.82 mg $Cm^{-3}$ $day^{-1}$ in anticyclonic eddy centers (18.5% and -15% relative to surroundings). All grazing pathways anomalies are either positive or insignificant for the difference between center, edge, and surroundings. This is consistent with an uplift (depression) of the nutricline in cyclonic and anticyclonic eddy centers. Zl grazing on Zs is 4.6% higher than the surroundings in cyclonic eddy centers (.04 mg $Cm^{-3}$ $day^{-1}$, 4.6%) and lower than the surroundings in anticyclonic eddy centers (-.1 mg $Cm^{-3}$ $day^{-1}$, -13.8%). Zp grazing on Zs are 18.1% higher in cyclonic eddy centers compared to surroundings with values of .03. Conversely, Zp grazing on Zs and Zl are 18.5% and 22.6% lower in anticyclonic eddy centers compared to surroundings. Along the edges, grazing in cyclonic and anticyclonic eddies is more similar to centers.

Case 4 eddies show biomass consistent with vertical motion at the edges resulting in enhanced or upward vertical mixing of the water column (Figure 13). Zs grazing on Ps has a biomass anomaly of 1.22 mg $Cm^{-3}$ $day^{-1}$ in cyclonic eddy centers and -.93 mg $Cm^{-3}$ $day^{-1}$ in anticyclonic eddy centers (28.9% and -21.7% relative to surroundings). Zl grazing on Zs is higher than the surroundings in cyclonic eddy centers and lower than the surroundings in anticyclonic eddy centers (.16 mg $Cm^{-3}$ $day^{-1}$, 18.8% and -.03 mg $Cm^{-3}$ $day^{-1}$, -4%). Zp grazing on Zs and Zl are higher in cyclonic eddy centers compared to surroundings (.05 mg $Cm^{-3}$ $day^{-1}$, 35.6% and .04 mg $Cm^{-3}$ $day^{-1}$, 19.3%). Conversely, Zp grazing on Zs and Zl anomalies are lower in anticyclonic eddy centers compared to surroundings. Along the edges, Zs grazing on Ps in cyclonic and anticyclonic eddies is 2.4 and .22 mg $Cm^{-3}$ $day^{-1}$which is 42.5% and 4.1% relative to the surroundings. Along cyclonic eddy edges, there is higher grazing difference relative to the surroundings in all pathways compared to anticyclonic eddy edges. Zp grazing on Zs has the second highest change in cyclonic edges with an increase of 25.6% (- 13.2% in anticyclones).

Note this is the case where eddies have the largest anomalies in MLD relative to surroundings so this may influence the anomalies for cyclonic eddy edges compared to anticyclonic eddy edges. See Table 1 for values.

Case 5 consists of eddies with lower Ps biomass at edges consistent with dilution or downward vertical mixing of the water column (Figure 14). Zs grazing on Ps has a biomass anomaly of 1 mg $Cm^{-3}$ $day^{-1}$ in cyclonic eddy centers and -.96 mg $Cm^{-3}$ $day^{-1}$in anticyclonic eddy centers (17.1% and -16.1% relative to surroundings). Zl grazing on Pl is different in cyclonic and anticyclonic eddy centers with a value of -.16 and -.13 which is 17% and 13% relative to the surroundings. Grazing is lower than in the center than surroundings for all grazing classes in both cyclonic and anticyclonic eddies. GrazZs2Zl is 6% lower than the surroundings in cyclonic eddy centers with a value of -.05 and 20% lower than the surroundings in anticyclonic eddy centers with a value of -.15 mg $Cm^{-3}$ $day^{-1}$. GrazPl2Zp is 19.7% lower than the surroundings in cyclonic eddy centers with a value of -.02 and 15.2% lower than the surroundings in anticyclonic eddy centers with a value of -.02 mg $Cm^{-3}$ $day^{-1}$. Zp grazing on Zs and Zl are 4% higher and 17.8% lower in cyclonic eddy centers compared to surroundings with values of .01 and -.04. Conversely, Zp grazing on Zs and Zl are 13.8% and 19.7% lower in anticyclonic eddy centers compared to surroundings. Case 5 eddies have minor changes in mixed layer depth between centers, edges and surroundings which could play a role in the modest changes across eddy centers and surroundings. Along the edges, GrazPs2Zs in cyclonic and anticyclonic eddies are .04 and -1.17 mg $Cm^{-3}$ $day^{-1}$ which is .6% and 19.6% relative to the surroundings. Only Ps biomass and NPP for Ps follow the dilution pattern at edges, suggesting that the top-down control is more important in setting biomass than dilution. Zp grazing on Zs and Zl have large anomalies in cyclonic edges (21.3%, 13.3% respectively). See Table 1 for values.

Table 1: Percent change in eddy centers and edges for each size class and grazing pathway compared to the eddy surroundings

| Var | Case 1 center | Case 1 edge | Case 2 center | Case 2 edge | Case 3 center | Case 3 edge | Case 4 center | Case 4 edge | Case 5 center | Case 5 edge | Eddy Type |
|---|---|---|---|---|---|---|---|---|---|---|---|
| Ps | 17.8% | 4.7% | -24.0% | -8.4% | -8.7% | -8.3% | -13.5% | 9.3% | -11.5% | -23.8% | Anticyclonic |
| | -14.2% | -2.6% | 30.3% | 9.3% | 11.5% | 11.4% | 12.4% | 29.0% | 13.4% | -6.9% | Cyclonic |
| NPPPs | 1.6% | -0.8% | -26.5% | -12.3% | -14.4% | -10.7% | -17.0% | 4.4% | -15.5% | -19.7% | Anticyclonic |
| | -2.4% | 3.4% | 35.8% | 16.1% | 18.0% | 15.5% | 26.0% | 40.7% | 16.8% | 0.2% | Cyclonic |
| Zs | -12.6% | -4.7% | -7.5% | -6.0% | -8.2% | -4.3% | -7.3% | -5.1% | -7.1% | 1.5% | Anticyclonic |
| | 14.6% | 6.4% | 10.9% | 8.9% | 10.4% | 6.9% | 16.0% | 14.1% | 7.6% | 7.4% | Cyclonic |
| Pl | -10.5% | 0.5% | 16.2% | 2.9% | -0.1% | 1.2% | 12.4% | -3.8% | 0.6% | 14.2% | Anticyclonic |
| | 6.3% | -1.8% | -9.6% | -3.3% | -2.7% | 0.5% | -3.7% | -9.5% | -9.5% | 4.2% | Cyclonic |
| NPPPl | -31.5% | -5.4% | 26.4% | 2.8% | -5.1% | 1.1% | 15.2% | -14.9% | -9.3% | 27.0% | Anticyclonic |
| | 27.5% | 2.6% | -22.0% | -3.4% | -6.4% | -4.5% | 0.6% | -19.8% | -15.7% | 12.2% | Cyclonic |
| Zl | -26.4% | -6.7% | 11.7% | -2.1% | -7.8% | -1.3% | 4.3% | -13.6% | -11.3% | 17.8% | Anticyclonic |
| | 29.2% | 5.9% | -14.5% | 0.3% | -0.8% | -1.7% | 5.8% | -12.4% | -8.4% | 13.7% | Cyclonic |
| Zp | -21.6% | -5.6% | 6.4% | -4.1% | -9.7% | -4.0% | 1.7% | -11.2% | -11.9% | 13.8% | Anticyclonic |
| | 27.3% | 6.2% | -2.0% | 4.9% | 5.8% | 4.1% | 12.7% | -1.1% | -3.6% | 13.1% | Cyclonic |
| Zs grazing on Ps | 0.7% | -1.2% | -26.9% | -12.7% | -15.0% | -10.9% | -16.9% | 4.1% | -16.1% | -19.6% | Anticyclonic |
| | -1.4% | 3.6% | 36.5% | 16.7% | 18.5% | 15.6% | 27.6% | 42.5% | 17.1% | 0.6% | Cyclonic |
| Zl grazing on Pl | -30.8% | -5.3% | 23.1% | 0.3% | -7.5% | -0.9% | 14.4% | -14.3% | -13.0% | 25.2% | Anticyclonic |
| | 29.6% | 3.7% | -22.4% | -3.3% | -5.7% | -3.9% | 1.5% | -20.5% | -17.0% | 13.4% | Cyclonic |
| Zl grazing on Zs | -31.9% | -9.8% | 3.4% | -7.6% | -13.8% | -5.3% | -3.5% | -16.9% | -19.9% | 15.0% | Anticyclonic |
| | 40.6% | 9.5% | -6.9% | 6.6% | 4.6% | 4.0% | 18.8% | -3.0% | -5.7% | 18.8% | Cyclonic |
| Zp grazing on Pl | -24.1% | 1.2% | 29.5% | 4.0% | -3.2% | 1.0% | 18.8% | -7.8% | -15.2% | 23.2% | Anticyclonic |
| | 13.7% | -3.8% | -22.1% | -6.6% | -11.0% | 2.1% | -4.6% | -18.1% | -19.7% | 5.1% | Cyclonic |
| Zp grazing on Zs | -27.1% | -9.2% | -8.0% | -13.1% | -18.5% | -10.4% | -10.7% | -13.2% | -13.8% | 12.0% | Anticyclonic |
| | 42.9% | 12.9% | 17.1% | 16.5% | 18.1% | 13.3% | 35.6% | 25.6% | 4.0% | 21.3% | Cyclonic |
| Zp grazing on Zl | -28.8% | -10.1% | -10.6% | -11.8% | -22.6% | -14.2% | -15.3% | -17.5% | -19.7% | 0.9% | Anticyclonic |
| | 33.5% | 6.6% | -6.7% | 3.5% | -9.1% | 5.4% | 19.3% | -8.4% | -17.8% | 13.3% | Cyclonic |
| MLD | 15.5% | 5.3% | 19.5% | 8.1% | 16.1% | 9.3% | 16.1% | 4.4% | 14.2% | 7.4% | Anticyclonic |
| | -13.5% | -9.6% | -16.6% | -13.1% | -15.9% | -13.1% | -18.9% | -19.5% | -13.8% | -10.1% | Cyclonic |

## *Discussion*

**Which physical dynamics in eddy centers impact plankton and productivity?**

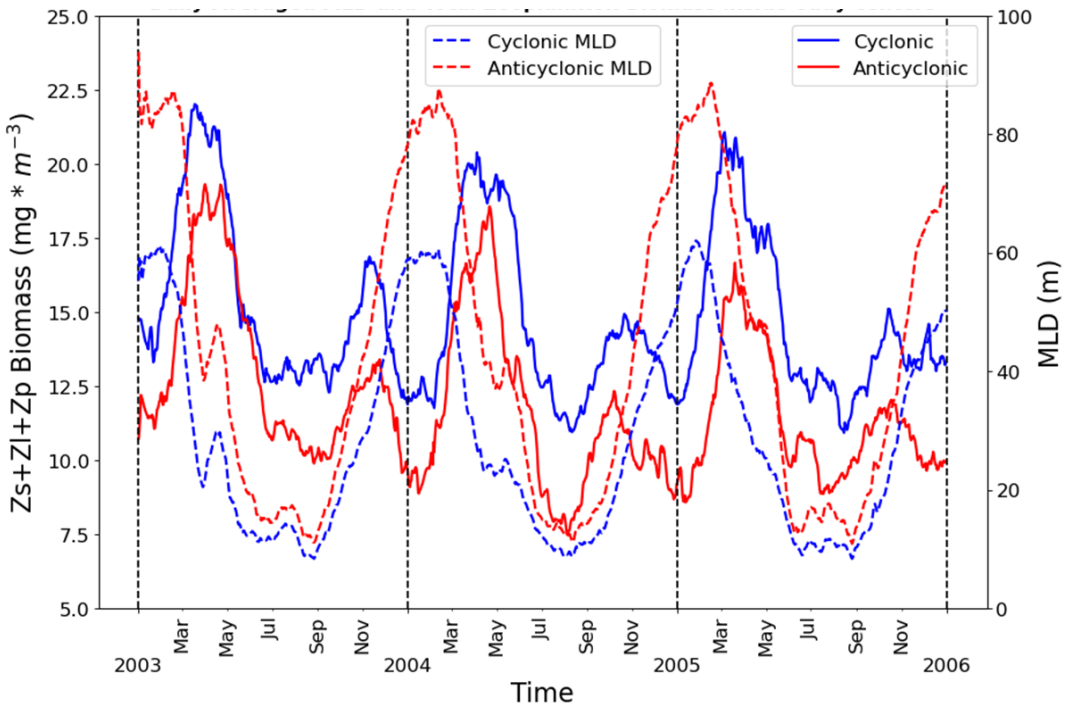


Figure 16: Seasonal change in anticyclonic (solid red) and cyclonic (solid blue) eddy center total zooplankton biomass and each eddies mixed layer depth in the center (dashed line)

Anticyclonic and cyclonic eddies differ due to the physical dynamics at play which impact the mixed layer depth. In a cyclonic eddy, the mixed layer depth is lowest within the center and gradually increases towards the edge, where the mixed layer depth is the same as the surrounding the eddy. Conversely, an anticyclonic eddy has the deepest mixed layer depth within the center and gradually decreases towards the edge and equals the surrounding mixed layer depth conditions. This uplift in cyclonic eddies and depression in anticyclonic eddies results in upwelling of cold, nutrient rich waters in cyclonic eddy centers and downwelling of warm, nutrient depleted waters in anticyclonic eddy centers. This pattern in mixed layer depth is evident

in the eddy data. Average cyclonic eddy mixed layer depth is 29.9 meters in the center, 31.3 meters along the edge and 35.7 meters surrounding the cyclonic eddies. Average anticyclonic eddy mixed layer depth is 44.3 meters in the center, 39.6 meters along the edge and 36.5 meters surrounding the anticyclonic eddies. The difference in mixed layer depth between cyclonic and anticyclonic eddy centers is 14.4 meters highlighting the significant role the physics of eddy centers play on nutrient pumping and on plankton NPP and biomass as the results show elevated biomass in cyclonic eddy centers and decreased biomass in anticyclonic eddy centers.

To further evaluate the role mixed layer depth plays in impacting plankton biomass within eddy centers, Figure 16 illustrates the seasonal pattern in mixed layer depth and total zooplankton biomass within eddy centers for both anticyclonic and cyclonic eddies. Mixed layer depth has an average depth of 81.1 meters in anticyclonic eddy centers and 52.8 meters in cyclonic eddy centers from December to February. Mixed layer depth is deepest in the winter because there is decreased stratification and increased wind driven mixing resulting in a deep mixed layer. However, in the spring, the mixed layer depth in anticyclonic eddy centers is 34.6 meters and 24.3 meters in cyclonic eddy centers. As temperatures increase in the GoM, the stratification intensifies as the warm surface layer separates from the cold bottom layer. The mixed layer depth is the shallowest in the summer with an average of 15.2 meters in anticyclonic eddy centers and 12.8 meters. Anticyclonic eddies and their center mixed layer depth (red solid line and red dotted line) show that as the mixed layer depth begins to shoal in spring, there is a delayed increase in total zooplankton biomass within anticyclonic eddy centers. This pattern is also evident in the cyclonic eddies with highest mixed layer depth in cyclonic eddy centers in February and March then an associated enhancement of total zooplankton biomass in late March to May. Furthermore, as the mixed layer depth continues to shoal in both anticyclonic and

cyclonic eddies as summer approaches, the total zooplankton biomass drops off again. This suggests that mixed layer depth and the general seasonality in the GoM of temperature and mixing are collectively impacting enhancement and dilution of total zooplankton biomass in eddy centers. In summer, the mixed layer is not deep enough to punch into the nutricline and bring nutrients to the surface which enables enhanced phytoplankton growth and increased phytoplankton grazing. Conversely in winter, there is decreased stratification, and the mixed layer depth can reach the nutricline allowing nutrients to move up to the surface and for increased light availability. This process and the associated growth in phytoplankton biomass followed by zooplankton biomass take time, leading to the delayed bloom in spring even as the mixed layer depth begins to shallow. This method of mixed layer depth controlling mesoscale eddies is also demonstrated globally by Gaube et al., 2019.

**Why does biomass and grazing differ in each eddy case along edge and center?**

Within each eddy case defined in section 3.4, the patterns in phytoplankton biomass and zooplankton biomass can vary due to the associated grazing and physical dynamics in each case. Figures 11 and 12 demonstrate highly geostrophic eddies and highly well mixed eddies, respectively. The geostrophic eddies in both anticyclonic and cyclonic eddies demonstrate large anomalies in the centers compared to the surroundings for small phytoplankton and NPP for small phytoplankton. Small zooplankton grazing is also high in both eddy types, but the small zooplankton biomass is not anomalous from the surrounding. This indicates that the small phytoplankton to small zooplankton grazing pathway is cycling rapidly. Furthermore, large phytoplankton biomass is anomalous, but the large phytoplankton growth is not anomalous. The grazing by large and predatory zooplankton on large phytoplankton is minimal so even though the large phytoplankton are not growing fast, they are escaping grazing pressure leading to

increased biomass. In cyclonic eddies, large zooplankton graze heavily on small zooplankton which applies tremendous grazing pressure on the small zooplankton and a lower biomass. Predatory zooplankton mainly graze on their largest prey available in large zooplankton. Overall, Case 2 eddies can be classified as being a single prey, linear grazing system and have the most productive and longest food web out of all the cases. The difference between edge and center for large and predatory zooplankton is lower compared to the lower trophic levels. This mechanism may be because zooplankton can more easily move vertically leading to a more distributed biomass across edge and center. Case 3, well mixed, eddies show similar patterns to case 2 except for the difference in biomass between center and edge is not anomalous. Also, as we increase in trophic levels, the difference between edge and center is enhanced which implies that the higher trophic levels are less subject to heavy horizontal mixing in these eddies. The patterns in grazing are like case 2 eddies as small, large, and predatory zooplankton prefer to graze on their largest prey available. Originally, we thought that Case 2 eddies and Case 3 eddies may behave differently. However, their biogeochemical and physical processes like speed and amplitude are similar suggesting that these two cases should be combined to form a case describing highly geostrophic eddies with high speeds, amplitudes, and long productive marine food webs.

Case 4 and 5 eddies (Figure 13 and 14) were meant to describe separate processes that could be happening along eddy edges. Case 4 eddies illustrate enhancement along the edges and case 5 eddies show dilution along the edges in both cyclonic and anticyclonic eddies based on the anomaly of small phytoplankton compared to the eddy surroundings. In case 4 anticyclonic eddies for small phytoplankton and growth, the edges see enhancement while the centers are less which is consistent with geostrophic dominance in the centers and ageostrophic vertical motions

along the edges which counteract the enhanced downwelling in centers. However, this dynamic does not propagate to the higher trophic levels as the zooplankton anomalies are negative for both edge and center. Compared to cases 1 through 3, anticyclonic eddies in case 4 have minimal grazing in small, large, and predatory zooplankton. In both case 4 anticyclonic and cyclonic eddies, large phytoplankton in eddy centers behave differently from the rest of the trophic levels. The large phytoplankton growth is negligible in both eddy types so the large phytoplankton is slowing trophic transfer to the higher trophic levels which may explain the behaviors in large and predatory zooplankton. Furthermore, the higher trophic levels in case 4 eddies behavior similar to case 2 and 3 eddies suggesting that whether we have strong geostrophic transport or instability resulting in ageostrophic vertical motions along the edges, the large and predatory zooplankton respond similarly.

For case 5 eddies (Figure 14), these are classified as having dilution at edges which is evident in both anticyclonic and cyclonic small phytoplankton biomass and growth. However, the anomalies in edge are opposite for large phytoplankton and all higher trophic levels suggesting that grazing may be responsible for the differences. Higher trophic levels in case 5 cyclonic eddies behave similarly to case 2, 3 and 4 cyclonic eddies. Small zooplankton biomass is not significantly different between the edge and center due to equal grazing pressure by large zooplankton. Because cyclonic edge biomass is higher for large and predatory zooplankton, we see an increased response in grazing propagating all the way to predatory zooplankton. It is important to note that the ratio of cyclonic eddies experiencing enhancement (case 4) is much lower than anticyclonic eddies and the opposite is true for dilution eddies (case 5) which shows more cyclonic eddies. This pattern may be the result of the edges counteracting motion within the center. While strong geostrophic upwelling is occurring with cyclonic eddy centers, there is

an opposite vertical downwelling at cyclonic edges resulting in more dilution. Conversely, strong downwelling in anticyclonic eddy centers results in upward vertical motions along edges resulting in more enhancement.

**Why is small phytoplankton biomass anomaly opposite from bottom-up hypothesis in many eddies?**

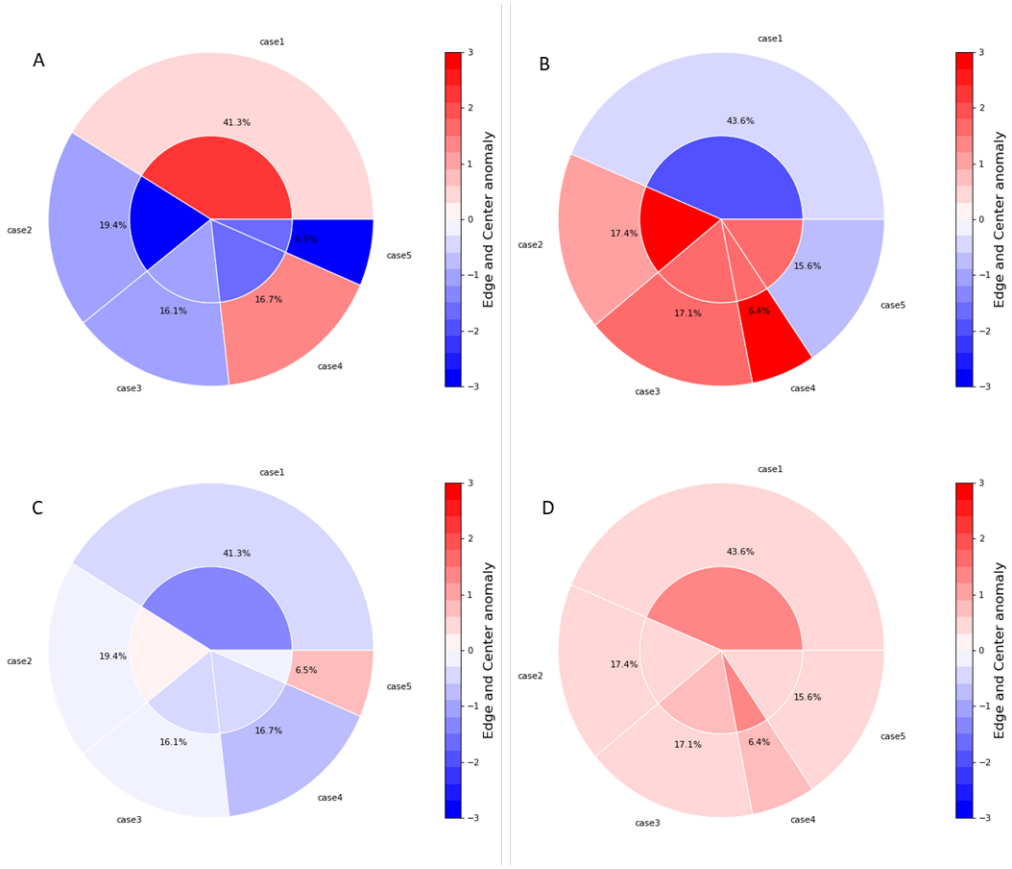


Figure 17: Anomalies of small phytoplankton (A & B) and small zooplankton biomass (C & D) for anticyclonic (A & C) and cyclonic (B & D) eddies as compared to the surrounding conditions. Inner circles of each panel show data for eddy centers, outer circles show eddy edges. Width of cases represents the percentage of occurrence for each case overall.

Figure 17 summarizes the center and edge anomaly for all cases for small phytoplankton biomass (anticyclonic: A, cyclonic: B) and small zooplankton biomass (anticyclonic: C, cyclonic: D). The inner circle represents the center anomaly and outer circle represents the edge

anomaly. 41.3% of anticyclonic eddies and 43.6% of cyclonic eddies have small phytoplankton biomass anomalies which differ from what we would expect (Case 1) with positive anomalies in anticyclonic centers and negative anomalies in cyclonic centers. We did not expect to see such a high percentage of anomalous eddies based on the bottom-up hypothesis. However, these same case 1 eddies for small zooplankton biomass (Figure 17 C & D) show center and edge anomalies which are consistent with our understanding of the physical dynamics occurring within each eddy center. This suggests that nutrient injection because of the eddies does not set the phytoplankton biomass but rather, zooplankton grazing may limit biomass.

To further examine this, we analyzed how total zooplankton biomass, total phytoplankton biomass, total grazing and total NPP changed with increasing amplitude within eddies for both cyclonic and anticyclonic eddy centers (Figure 18). We expect eddies with larger amplitudes to have larger nutricline displacements, larger nutrient fluxes, and hence greater anomalies. However, total phytoplankton biomass does not show a significant slope with increasing amplitude, indicated by the central light blue (cyclonic) and light red (anticyclonic) lines. Rates of NPP, and total zooplankton grazing, and biomass have increased with increasing amplitude which suggests that eddy nutrient supply more strongly affects the zooplankton biomass and grazing. This would indicate that instead of a bottom-up approach, eddies in the oligotrophic GoM experience top-down control of biomass while still cycling rapidly.

After analyzing the phytoplankton and zooplankton biomass and associated grazing within each eddy case we defined, we find that the separate mechanisms in each case have a greater impact on the lower trophic levels (small phytoplankton, large phytoplankton, small zooplankton, and phytoplankton growth) compared to the higher trophic levels (large and predatory zooplankton). However, the impacts on biomass are inconsistent with physical impacts

caused by the eddies. This indicates that the separate cases are actually describing biologically different systems rather than illustrating the physical dynamics when assuming bottom-up control. Therefore, we conclude that applying a bottom-up approach using small phytoplankton biomass as the predictor of varying eddy dynamics impacting biomass and trophic transfer may not be the best approach and utilizing zooplankton biomass may better explain the impacts of eddy centers and edges on trophic transfer and biomass in the oligotrophic GoM.

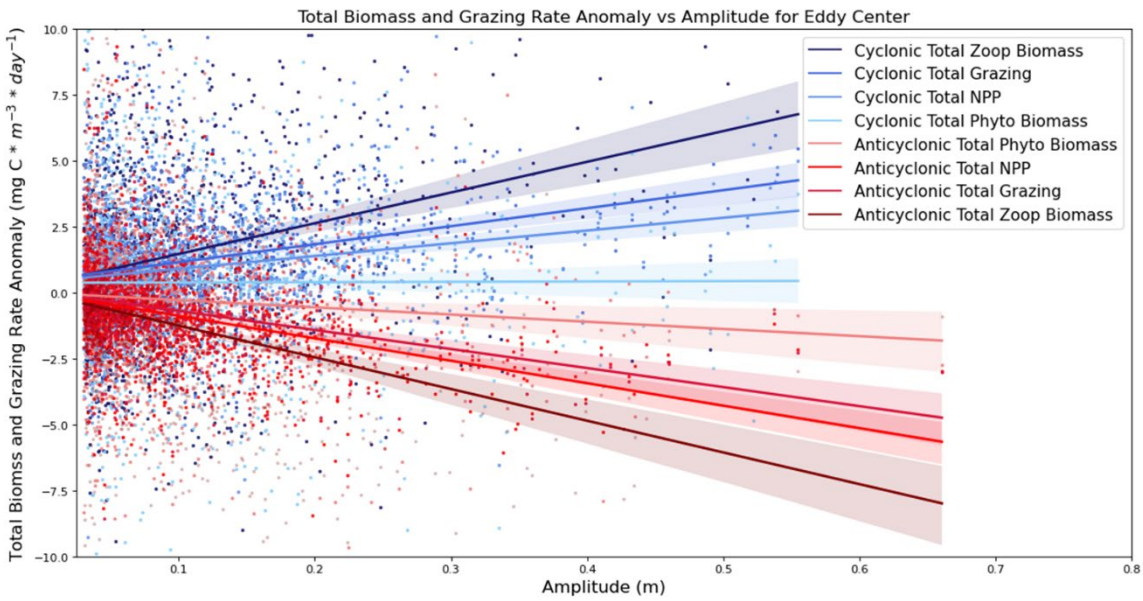


Figure 18: Total phytoplankton and zooplankton biomass, NPP, and grazing anomaly vs eddy amplitude for anticyclonic and cyclonic eddies

**Implications of grazing and what it tells us about trophic transfer in the Gulf of Mexico**

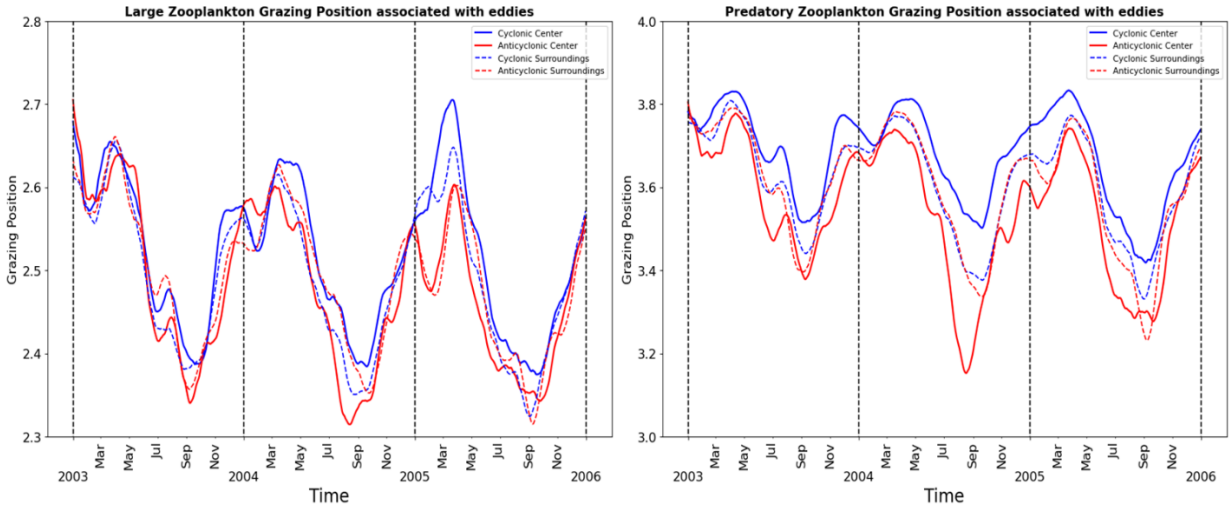


Figure 19: Large and predatory zooplankton grazing position associated with eddy center, edges and surrounding for anticyclonic and cyclonic eddies across the entire time series

The grazing position for each individual eddy case was not significantly different. However, we found that the grazing position differed between anticyclonic and cyclonic eddy centers, edges, and surroundings. Also, on a seasonal basis, small, large, and predatory zooplankton grazing behaviors change in the oligotrophic GoM. Figure 18 illustrates the seasonal grazing position for large zooplankton (Figure 19A) and predatory zooplankton (Figure 19B) for cyclonic and anticyclonic eddy centers, edges, and surroundings. For large zooplankton, a grazing position of 2 means large zooplankton is exclusively grazing on large phytoplankton and a grazing position of 3 means large zooplankton is exclusively grazing on small zooplankton. For predatory zooplankton, a grazing position of 3 means predatory zooplankton is exclusively grazing on small zooplankton and a grazing position of 4 means predatory zooplankton is exclusively grazing on large zooplankton. Seasonally, the average grazing position for predatory zooplankton is never less than 3 indicating that predatory zooplankton grazing on large phytoplankton is minimal. This is consistent with the low large phytoplankton

biomass in eddy centers compared to small phytoplankton and small, large, and predatory zooplankton. Cyclonic and anticyclonic centers are bolded in the figure to better represent the difference between the two eddy types. Overall, the grazing trophic position for anticyclonic and cyclonic eddy edges and surroundings is confined by eddy centers. Cyclonic eddy centers have the highest grazing position while anticyclonic eddy centers have the lowest grazing position for both large and predatory zooplankton. For both large and predatory zooplankton, the grazing position is highest in the spring and lowest in the summer. This suggests that the marine food web within both eddy types is more productive, and the food web is longer in the spring as zooplankton graze more on the largest prey available (Negrete-García et al., 2022; Ryther, 1969). Also, large, and predatory zooplankton are selective feeders in the spring as there is more biomass so they can choose to eat the largest prey for higher efficiency. Conversely in summer, the eddies are less productive in terms of grazing and large and predatory zooplankton will eat what is available to them even if the prey is smaller. These patterns in grazing position are consistent with our understanding of the seasonality of phytoplankton and zooplankton biomass. Even in the oligotrophic GoM, this implies that productivity within eddies is important for phytoplankton and zooplankton growth and there are changes in zooplankton feeding in the less productive oligotrophic GoM just like you would see in the more productive continental shelf.

# Chapter 3: Conclusions

By solving a series of equations from a physical-biogeochemical model, we estimate zooplankton biomass and grazing throughout the GoM from satellite-derived temperature, phytoplankton biomass, and NPP. The distribution of zooplankton biomass is elevated not only on the shelf but also in regions of the oligotrophic GoM, especially around the Loop Current. Anticyclonic and cyclonic eddies were detected from a Py-Eddy-Tracker software using SSH, and eastward and northward sea water velocity. The algorithm detected 11,240 cyclonic and 9,698 anticyclonic eddies from 2003 through 2006. On average, about 32% of the oligotrophic GoM is occupied by an eddy on any given day suggesting that they have a substantial impact on biomass and grazing in this region. Cyclonic eddy centers had positive biomass and grazing anomalies from the surroundings while anticyclonic eddy centers had negative anomalies from the surroundings. The basin average zooplankton biomass lies intermediate between the cyclonic and anticyclonic eddy centers indicating the positive and negative impact the eddies are having on biomass and grazing in the GoM. Edge effects are evident in both eddy types with more cyclonic eddies experiencing dilution at the edges while more anticyclonic eddies experience enhancement at the edge. Zooplankton grazing follows similar patterns to biomass in eddy centers and edges and large and predatory zooplankton graze mostly on the largest prey available to them (small zooplankton and large zooplankton respectively). In the spring, the zooplankton graze selectively on the large prey available when biomass is higher but in the summer, the zooplankton graze on any prey available when biomass is low. Originally, we divided the eddies into 5 cases based on small phytoplankton biomass assuming a bottom-up control. We expected to see changes in biomass due to varying physical dynamics occurring within each case. However, we found that the cases were biologically descriptive instead of physically descriptive.

Furthermore, 41% of anticyclonic and 44% of cyclonic eddies had anomalous centers based on small phytoplankton biomass. However, these same anomalous eddies followed the expected increases and decreases in eddy centers when looking at small zooplankton biomass. Therefore, we conclude that nutrient supply does not drive phytoplankton biomass and, rather, zooplankton grazing may often limit accumulation of phytoplankton biomass**. Thus, many GoM eddies are experiencing top-down control.** An understanding of small-scale zooplankton dynamics in the oligotrophic ocean may enhance the fisheries literature by revealing unexplored areas where we may see increased fish reproduction and grazing. Advances in remote sensing that allow the discrimination of phytoplankton functional types, like the new PACE satellite, will be useful for providing a more complete base of the food web and thus enhance estimation of zooplankton biomass.

# Appendices

## Methods:

### Physical-Biogeochemical Model

An existing, validated coupled physical-biogeochemical model (Shropshire et al., 2020) is used both as the basis and validation for our zooplankton estimates. The biogeochemical model (NEMURO-GoM) was originally developed for the North Pacific but has been re-parametrized and validated to imply the physical dynamics of the Gulf of Mexico using both historical and new observations (Shropshire et al., 2020). The North Pacific Ecosystem Model for Understanding Regional Oceanography (NEMURO) is an ecosystem model that describes the relationships between lower and upper trophic levels. The model consists of eleven state variables which include nitrate, ammonium, particulate and dissolved nitrogen, particulate silica, silicic acid concentration, two size classes of phytoplankton (small and large P) and three size classes of zooplankton (small, large, and predatory Z) (Kishi et al., 2007). To implement the North Pacific formulation of NEMURO model in the Gulf of Mexico, several adjustments were made to both parameters and the model structure. The first adjustment was to remove the ability for large zooplankton to graze on the model small phytoplankton because in the Gulf of Mexico, small phytoplankton are dominated by cyanobacteria which are too small for larger zooplankton to graze. Also, mortality was changed to be linear for all state variables except predatory zooplankton. The NEMURO-GoM ecosystem model was an appropriate choice because it focuses on the zooplankton community by including three different zooplankton size classes. This allows us to examine zooplankton dynamics more in depth than many other biogeochemical models. The NEMURO-GoM biogeochemical model is imbedded in a physical Hybrid Coordinate Ocean Model (HYCOM) model which is described next.

HYCOM uses flexible vertical coordinates that are fixed vertical levels in the upper ocean, isopycnal in the ocean interior and depth following along coastal regions and shelves (Chassignet et al., 2003). The HYCOM-GoM has a spatial resolution of about 4 kilometers and the model assimilates satellite altimeter observations, satellite and in-situ SST observation and vertical temperature and salinity profiles from Argo floats. The model provides SSH fields used for obtaining estimates of both anticyclonic and cyclonic eddies. Mixed layer depth was obtained from HYCOM and used for estimation of the vertically integrated NPP.

The NEMURO-GoM model uses mechanistic equations describing the changes in small and large phytoplankton and small, large, and predatory zooplankton biomass resulting from growth and mortality. The physical model then advects and diffuses the community throughout the domain. The zooplankton grazing terms represent one form of mortality for the phytoplankton groups. Given fields of temperature, phytoplankton biomass and its partitioning between large and small groups, net primary productivity (NPP) and mixed layer depth, coupled with the assumption of steady state biomass, the phytoplankton equations from the model can be used to estimate zooplankton and grazing in the Gulf of Mexico from satellite derived products (Coles, Atkinson, Huebert, Pierson, Rose, Chaichitehrani, in prep). We apply this technique to remote sensing data in the Gulf of Mexico.

**Eddy detection Algorithm**

The algorithm was implemented to investigate eddy impacts within the Brazil-Malvinas Confluence, in the South Atlantic (Mason et al., 2017). Thus, the algorithm criteria for detecting mesoscale and sub mesoscale eddies needed to be evaluated for application to the latitude and specific physical dynamics of the Gulf of Mexico. A sensitivity analysis was conducted by

individually varying the criteria used to detect eddies to determine their effect on eddy detection. Stationary images throughout a year were created for each parameter variation to visualize how the adjustments affected eddy detection. The following details the sensitivity of each parameter.

The first parameter evaluated was the use of the Bessel high pass filter on the SSH. This filter, designed to remove spatial variability at large scales to highlight the eddy variations, was set to a wavelength of five hundred kilometers and an order of three. Even at the small scale of the GOM, the filter smoothed the SSH data, improving eddy detection in the Gulf of Mexico, so the default parameter was retained. Next, the algorithm criterion which allows for a shape error of the eddy boundary relative to a perfect circle contour was evaluated. Decreasing the shape error parameter causes the algorithm to falsely detect SSH contours throughout the entire Gulf of Mexico basin as eddies. The algorithm detected more eddies when the shape error was decreased from 55% to 40% but the new detections exhibited an elongated and narrow shape that was visually inconsistent with the horizontal structure of an eddy. Increasing the shape error parameter beyond 70% resulted in the removal of eddies that were visually determined to be suitable for this research. So, the shape error was slightly adjusted from 55% to 60%. The criterion for the minimum number of SSH pixels inside a contour needed to be considered an eddy was then varied. When adjusting the original maximum and minimum SSH pixel limits (8 to 1000), there were large anticyclonic eddies greater than 1000 pixels not being detected. Therefore, the maximum SSH pixel limit was changed to 20000 to ensure any mesoscale eddies that meet the other criterion in the GoM are detected.

Overall, these parameters' variability did not have large effects on the eddy detection and the algorithm was still missing key Loop Current eddies at some time periods. Because the anticyclonic eddies shed off the Loop Current in the Gulf of Mexico tend to be quite large

(Brokaw et al., 2020), we next adjusted the amplitude threshold parameters. The 3 parameters controlling the amplitude threshold consist of the maximum number of local extrema (MNLE) within the contour, the minimum number of steps of intervals of sea surface height to consider in the eddy detection, and the number of intervals to be considered as another extrema. After visual inspections of 2 randomly selected days each month from 2003 to 2006, there was little to no impact on the number of eddies detected when changing the number of intervals to be considered as another extrema. Increasing the minimum number of steps between contours for eddy detection reduced the number of eddies by removing some of the small eddies with a radius less than 2 kilometer that were considered unlikely to be resolved well in the satellite data.

The adjustment of the MNLE within a contour had the greatest impact on eddy detection. Originally, the MNLE was set to 1. Figure 2 contrasts MNLE parameters that vary from 1 (Figure 2A) to 4 (Figure 2B) The black rectangle on Figure 3A surrounds an anticyclonic eddy which is not detected until the MNLE reaches 4. The adjusted algorithm also detects a suspected cyclonic eddy at 92°W and 26°N that went previously undetected. After investigating each parameter in isolation, the revised values were combined to create the new algorithm which better represents the physical dynamics of eddies and fronts in the Gulf of Mexico. To further validate the improvements in the adjusted algorithm, visual analysis was conducted to determine the changes in false positives and false negatives between the original algorithm and the adjusted algorithm. Two equally spaced days per month were visually evaluated to count the number of false positives and false negatives from each algorithm version. False positives were defined as eddies the algorithm detected but did not display the usual characteristics of an eddy and false negatives were eddies that exhibited the characteristics of an eddy but were not detected by the algorithm. The number of anticyclonic false positives were reduced by 55% from 124 to 56 and

the number of anticyclonic false negatives were reduced by 70% from 148 to 44 using the new parameter set. The number of cyclonic false positives was reduced by 34% from 128 to 84 and the number of cyclonic false negatives was reduced by 58% from 172 to 72 with the revised parameters. The greatest improvement in the algorithm results from detecting more anticyclonic eddies which is ideal as we want to capture the Loop Current eddies (Brokaw et al., 2020).

**Temporal variations in eddy parameters**

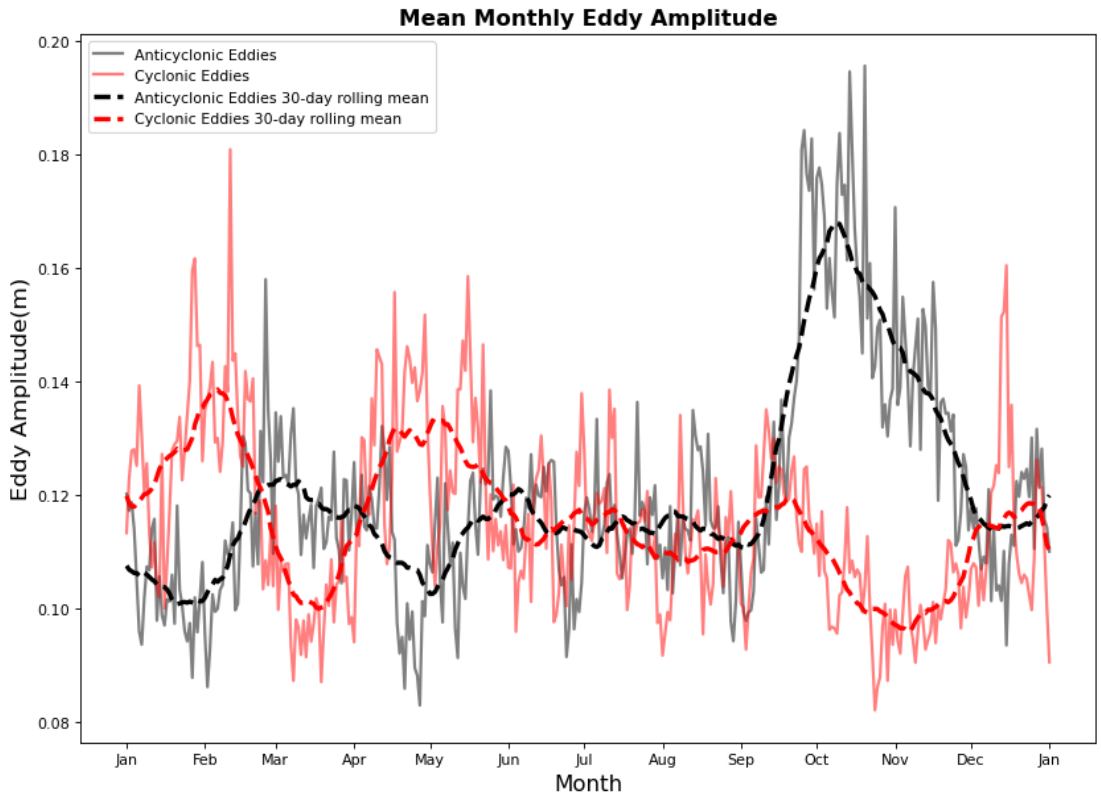


Figure S1: Monthly averaged eddy amplitude for cyclonic (red) and anticyclonic (black) eddies

The mean amplitude of anticyclones and cyclones across the year is relatively constant (Figure S1). However, a 23% increase in mean anticyclonic amplitude occurs in Fall compared to the rest of the year which was not observed by Zhu & Liang 2022, indicating that this increase

may be due to the shorter period this study sampled. Mean cyclonic amplitude is nearly uniform from June to October but is highest in February and May and lowest in November.

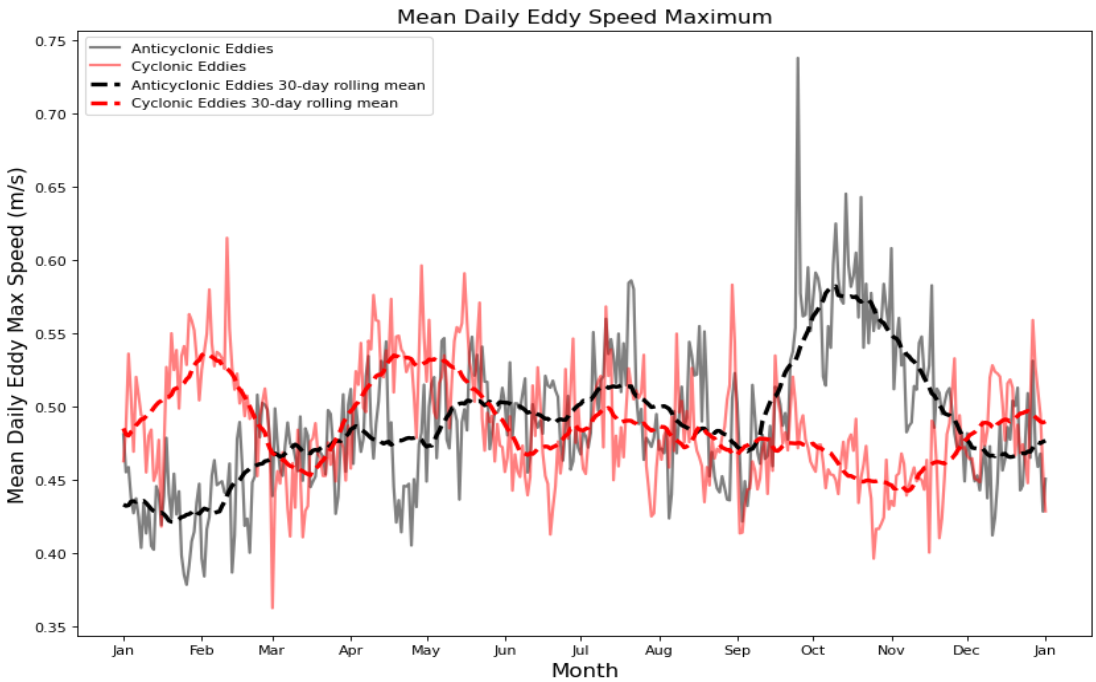


Figure S2: Monthly averaged eddy maximum speed for cyclonic (red) and anticyclonic (black) eddies

Monthly averaged maximum speed within an eddy (Figure S2) mirrors amplitude closely as is expected, being slightly higher within anticyclonic eddies from June to December and higher within cyclonic eddies from December to June. The mean maximum speed is mostly uniform throughout the year with a difference between the maximum and minimum average speed of .13 m/s and .1 m/s for anticyclonic and cyclonic eddies which is 23% and 19% of the overall maximum speed, respectively.

# Bibliography


Behrenfeld, M. J., Boss, E., Siegel, D. A., & Shea, D. M. (2005). Carbon-based ocean productivity and phytoplankton physiology from space. *Global Biogeochemical Cycles*, *19*(1), 1–14. https://doi.org/10.1029/2004GB002299

Biggs, D. C., & Ressler, P. H. (2001a). Distribution and Abundance of Phytoplankton, Zooplankton, Distribution and Abundance of Phytoplankton, Zooplankton, Ichthyoplankton, and Micronekton in the Deepwater Gulf of Ichthyoplankton, and Micronekton in the Deepwater Gulf of Mexico Mexico. *Gulf of Mexico Science*, *19*. https://doi.org/10.18785/goms.1901.02

Biggs, D. C., & Ressler, P. H. (2001b). Distribution and abundance of phytoplankton, zooplankton, ichthyoplankton, and micronekton in deepwater Gulf of Mexico. *Gulf of Mexico Science*, *19*(1), 7–29. https://doi.org/10.18785/goms.1901.02

Brokaw, R. J., Subrahmanyam, B., Trott, C. B., & Chaigneau, A. (2020). Eddy Surface Characteristics and Vertical Structure in the Gulf of Mexico from Satellite Observations and Model Simulations. *Journal of Geophysical Research: Oceans*, *125*(2). https://doi.org/10.1029/2019JC015538

Callejas-Jimenez, M., Santamaria-del-Angel, E., Gonzalez-Silvera, A., Millan-Nuñez, R., & Cajal-Medrano, R. (2012). Dynamic Regionalization of the Gulf of Mexico based on normalized radiances (nLw) derived from MODIS-Aqua. *Continental Shelf Research*, *37*, 8–14. https://doi.org/10.1016/J.CSR.2012.01.014

Carvalho, A. da C. de O., Mendes, C. R. B., Kerr, R., Azevedo, J. L. L. de, Galdino, F., & Tavano, V. M. (2019). The impact of mesoscale eddies on the phytoplankton community in the South Atlantic Ocean: HPLC-CHEMTAX approach. *Marine Environmental Research*, *144*, 154–165. https://doi.org/10.1016/J.MARENVRES.2018.12.003

Chassignet, E. P., Smith, L. T., Halliwell, G. R., & Bleck, R. (n.d.). *North Atlantic Simulations with the Hybrid Coordinate Ocean Model (HYCOM): Impact of the Vertical Coordinate Choice, Reference Pressure, and Thermobaricity*. http://hycom.

Chelton, D. B., Schlax, M. G., & Samelson, R. M. (2011). Global observations of nonlinear mesoscale eddies. *Progress in Oceanography*, *91*(2), 167–216. https://doi.org/10.1016/j.pocean.2011.01.002

Cruz-Rosado, L., Contreras-Sánchez, W. M., Hernández-Vidal, U., Gómez-Gutiérrez, J., Contreras-García, M. de J., & McDonal-Vera, A. (2020). Seasonal variability of near-surface zooplankton

community structure in the southern Gulf of Mexico. *Latin American Journal of Aquatic Research*, *48*(4), 649–661. https://doi.org/10.3856/vol48-issue4-fulltext-2503

Damien, P., Sheinbaum, J., Pasqueron De Fommervault, O., Jouanno, J., Linacre, L., & Duteil, O. (2021). Do Loop Current eddies stimulate productivity in the Gulf of Mexico? *Biogeosciences*, *18*(14), 4281–4303. https://doi.org/10.5194/bg-18-4281-2021

Douglass, E. M., & Richman, J. G. (2015). Analysis of ageostrophy in strong surface eddies in the Atlantic Ocean. *Journal of Geophysical Research: Oceans*, *120*(3), 1490–1507. https://doi.org/10.1002/2014JC010350

Elliott, D. T., Pierson, J. J., & Roman, M. R. (2012). Relationship between environmental conditions and zooplankton community structure during summer hypoxia in the northern Gulf of Mexico. *Journal of Plankton Research*, *34*(7), 602–613. https://doi.org/10.1093/plankt/fbs029

Franks, P. J. S., Wroblewski, J. S., & Flierl, G. R. (1986). Prediction of phytoplankton growth in response to the frictional decay of a warm-core ring. *Journal of Geophysical Research: Oceans*, *91*(C6), 7603–7610. https://doi.org/10.1029/jc091ic06p07603

Gaube, P., Chelton, D. B., Strutton, P. G., & Behrenfeld, M. J. (2013). Satellite observations of chlorophyll, phytoplankton biomass, and Ekman pumping in nonlinear mesoscale eddies. *Journal of Geophysical Research: Oceans*, *118*(12), 6349–6370. https://doi.org/10.1002/2013JC009027

Gaube, P., J. McGillicuddy, D., & Moulin, A. J. (2019). Mesoscale Eddies Modulate Mixed Layer Depth Globally. *Geophysical Research Letters*, *46*(3), 1505–1512. https://doi.org/10.1029/2018GL080006

Gaube, P., McGillicuddy, D. J., Chelton, D. B., Behrenfeld, M. J., & Strutton, P. G. (2014). Regional variations in the influence of mesoscale eddies on near-surface chlorophyll. *Journal of Geophysical Research: Oceans*, *119*(12), 8195–8220. https://doi.org/10.1002/2014JC010111

Gomez, F. A., Lee, S. K., Liu, Y., Hernandez, F. J., Muller-Karger, F. E., & Lamkin, J. T. (2018). Seasonal patterns in phytoplankton biomass across the northern and deep Gulf of Mexico: A numerical model study. *Biogeosciences*, *15*(11), 3561–3576. https://doi.org/10.5194/BG-15-3561-2018

Gower, J. F. R., Denman, K. L., & Holyer, R. J. (1980). Phytoplankton patchiness indicates the fluctuation spectrum of mesoscale oceanic structure. *Nature 1980 288:5787*, *288*(5787), 157–159. https://doi.org/10.1038/288157a0

Guerrero, L., Sheinbaum, J., Mariño-Tapia, I., González-Rejón, J. J., & Pérez-Brunius, P. (2020). Influence of mesoscale eddies on cross-shelf exchange in the western Gulf of Mexico. *Continental Shelf Research*, *209*. https://doi.org/10.1016/J.CSR.2020.104243

Hiron, L., Miron, P., Shay, L. K., Johns, W. E., Chassignet, E. P., & Bozec, A. (2022). Lagrangian coherence and source of water of Loop Current Frontal Eddies in the Gulf of Mexico. *Progress in Oceanography*, *208*, 102876. https://doi.org/10.1016/J.POCEAN.2022.102876

Jiawei Zhuang, raphael dussin, David Huard, Pascal Bourgault, Anderson Banihirwe, Stephane Raynaud, Brewster Malevich, Martin Schupfner, Filipe, Sam Levang, Charles Gauthier, André Jüling, Mattia Almansi, RichardScottOZ, RondeauG, Stephan Rasp, Trevor James Smith, Jemma Stachelek, Matthew Plough, … Xianxiang Li. (2023). pangeo-data/xESMF: v0.8.2 (v0.8.2). Zenodo. https://doi.org/10.5281/zenodo.835679

Kishi, M. J., Kashiwai, M., Ware, D. M., Megrey, B. A., Eslinger, D. L., Werner, F. E., Noguchi-Aita, M., Azumaya, T., Fujii, M., Hashimoto, S., Huang, D., Iizumi, H., Ishida, Y., Kang, S., Kantakov, G. A., Kim, H. cheol, Komatsu, K., Navrotsky, V. V., Smith, S. L., … Zvalinsky, V. I. (2007). NEMURO-a lower trophic level model for the North Pacific marine ecosystem. *Ecological Modelling*, *202*(1–2), 12–25. https://doi.org/10.1016/j.ecolmodel.2006.08.021

Le Hénaff, M., Kourafalou, V. H., Morel, Y., & Srinivasan, A. (2012). Simulating the dynamics and intensification of cyclonic Loop Current Frontal Eddies in the Gulf of Mexico. *Journal of Geophysical Research: Oceans*, *117*(2). https://doi.org/10.1029/2011JC007279

Li, G., Wang, Z., & Wang, B. (2022). Multidecade Trends of Sea Surface Temperature, Chlorophyll-a Concentration, and Ocean Eddies in the Gulf of Mexico. *Remote Sensing 2022, Vol. 14, Page 3754*, *14*(15), 3754. https://doi.org/10.3390/RS14153754

Liu, X., & Levine, N. M. (2016). Enhancement of phytoplankton chlorophyll by submesoscale frontal dynamics in the North Pacific Subtropical Gyre. *Geophysical Research Letters*, *43*(4), 1651–1659. https://doi.org/10.1002/2015GL066996

Mahadevan, A. (2016). The Impact of Submesoscale Physics on Primary Productivity of Plankton. *Annual Review of Marine Science*, *8*, 161–184. https://doi.org/10.1146/annurev-marine-010814-015912

Mahadevan, A., Thomas, L. N., & Tandon, A. (2008). Comment on "eddy/wind interactions stimulate extraordinary mid-ocean plankton blooms." In *Science* (Vol. 320, Issue 5875). https://doi.org/10.1126/science.1152111

Martinez, M. A., Hereu, C. M., Arteaga, M. C., Jiménez-Rosenberg, S. P. A., Herzka, S. Z., Saavedra-Flores, A., Robles-Flores, J., Gomez-Reyes, R., Batta-Lona, P. G., Gasca-Pineda, J., & Galindo-Sánchez, C. E. (2021). Epipelagic zooplankton diversity in the deep water region of the Gulf of Mexico: A metabarcoding survey. *ICES Journal of Marine Science*, *78*(9), 3317–3332. https://doi.org/10.1093/icesjms/fsab090

Martínez-López, B., & Zavala-Hidalgo, J. (2009). Seasonal and interannual variability of cross-shelf transports of chlorophyll in the Gulf of Mexico. *Journal of Marine Systems*, *77*(1–2), 1–20. https://doi.org/10.1016/J.JMARSYS.2008.10.002

Mason, E., Pascual, A., Gaube, P., Ruiz, S., Pelegrí, J. L., & Delepoulle, A. (2017). Subregional characterization of mesoscale eddies across the Brazil-Malvinas Confluence. *Journal of Geophysical Research: Oceans*, *122*(4), 3329–3357. https://doi.org/10.1002/2016JC012611

Mason, E., Pascual, A., & McWilliams, J. C. (2014). A new sea surface height-based code for oceanic mesoscale eddy tracking. *Journal of Atmospheric and Oceanic Technology*, *31*(5), 1181–1188. https://doi.org/10.1175/JTECH-D-14-00019.1

McGillicuddy, D. J. (2016). Mechanisms of Physical-Biological-Biogeochemical Interaction at the Oceanic Mesoscale. *Annual Review of Marine Science*, *8*, 125–159. https://doi.org/10.1146/annurev-marine-010814-015606

McGillicuddy, D. J., Anderson, L. A., Bates, N. R., Bibby, T., Buesseler, K. O., Carlson, C. A., Davis, C. S., Ewart, C., Falkowski, P. G., Goldthwait, S. A., Hansell, D. A., Jenkins, W. J., Johnson, R., Kosnyrev, V. K., Ledwell, J. R., Li, Q. P., Siegel, D. A., & Steinberg, D. K. (2007). Eddy/Wind interactions stimulate extraordinary mid-ocean plankton blooms. *Science*, *316*(5827), 1021–1026. https://doi.org/10.1126/science.1136256

Meunier, T., Pallás-Sanz, E., Tenreiro, M., Portela, E., Ochoa, J., Ruiz-Angulo, A., & Cusí, S. (2018). The Vertical Structure of a Loop Current Eddy. *Journal of Geophysical Research: Oceans*, *123*(9), 6070–6090. https://doi.org/10.1029/2018JC013801

Morey, S. L., Dukhovskoy, D. S., & Bourassa, M. A. (2009). Connectivity of the Apalachicola River flow variability and the physical and bio-optical oceanic properties of the northern West Florida Shelf. *Continental Shelf Research*, *29*(9), 1264–1275. https://doi.org/10.1016/j.csr.2009.02.003

Mouw, C. B., & Yoder, J. A. (2010). Optical determination of phytoplankton size composition from global SeaWiFS imagery. *Journal of Geophysical Research: Oceans*, *115*(12). https://doi.org/10.1029/2010JC006337

Muller-Karger, F. E. (2000). The spring 1998 northeastern Gulf of Mexico (NEGOM) cold water event: Remote sensing evidence for upwelling and for eastward advection of Mississippi water (or: How an errant loop current anticyclone took the NEGOM for a spin). *Gulf of Mexico Science*, *18*(1), 55–67. https://doi.org/10.18785/goms.1801.06

Muller-Karger, F. E., Smith, J. P., Werner, S., Chen, R., Roffer, M., Liu, Y., Muhling, B., Lindo-Atichati, D., Lamkin, J., Cerdeira-Estrada, S., & Enfield, D. B. (2015). Natural variability of surface oceanographic conditions in the offshore Gulf of Mexico. *Progress in Oceanography*, *134*, 54–76. https://doi.org/10.1016/j.pocean.2014.12.007

Nacional, U., De, A., México, M., Morales, S., Gasca, E. ;, Segura, R. ;, & Biggs, L. ; (2002). Planktonic cnidarians in a cold-core ring in the Gulf of Mexico Anales del Instituto de Biología. *Serie Zoología*, *73*(1), 19–36. http://www.redalyc.org/articulo.oa?id=45873103

NASA OBPG. (2020). *MODIS Aqua Global Level 3 Mapped SST. Ver. 2019.0. PO.DAAC, CA, USA. Dataset accessed [2022-10-18] at https://doi.org/10.5067/MODSA-1D4D9*.

Negrete-García, G., Luo, J. Y., Long, M. C., Lindsay, K., Levy, M., & Barton, A. D. (2022). Plankton energy flows using a global size-structured and trait-based model. *Progress in Oceanography*, *209*. https://doi.org/10.6075/J0NK

Olvera-Prado, E. R., Romero-Centeno, R., Zavala-Hidalgo, J., Moreles, E., & Ruiz-Angulo, A. (2023). Contribution of the wind, Loop Current Eddies, and topography to the circulation in the southern Gulf of Mexico. *Ocean Dynamics*, *73*(10), 597–618. https://doi.org/10.1007/s10236-023-01569-5

Pingree, R. D., Holligan, P. M., & Mardell, G. T. (1979). Phytoplankton growth and cyclonic eddies. *Nature 1979 278:5701*, *278*(5701), 245–247. https://doi.org/10.1038/278245a0

Ryther, J. H. (1969). Photosynthesis and fish production in the sea. *Science*, *166*(3901), 72–76. https://doi.org/10.1126/SCIENCE.166.3901.72/ASSET/E4964C91-AA50-4E7E-9B1A-E93469321762/ASSETS/SCIENCE.166.3901.72.FP.PNG

Salmerón-García, O., Zavala-Hidalgo, J., Mateos-Jasso, A., & Romero-Centeno, R. (2011). Regionalization of the gulf of mexico from space-time chlorophyll-a concentration variability. *Ocean Dynamics*, *61*(4), 439–448. https://doi.org/10.1007/s10236-010-0368-1

Samuelsen, A., Hjøllo, S. S., Johannessen, J. A., & Patel, R. (2012). Particle aggregation at the edges of anticyclonic eddies and implications for distribution of biomass. *Ocean Science*, *8*(3), 389–400. https://doi.org/10.5194/os-8-389-2012

Sánchez-Mejiá, J. M., Monreal-Gómez, M. A., Durán-Campos, E., Salas De León, D. A., Coria-Monter, E., Contreras-Simuta, M. G., & Merino-Ibarra, M. (2020). Impact of a Mesoscale Cyclonic Eddy on the Phytoplankton Biomass of Bay of la Paz in the Southern Gulf of California. *Pacific Science*, *74*(4), 331–344. https://doi.org/10.2984/74.4.2

Sánchez-Velasco, L., Lavín, M. F., Jiménez-Rosenberg, S. P. A., Godínez, V. M., Santamaría-del-Angel, E., & Hernández-Becerril, D. U. (2013). Three-dimensional distribution of fish larvae in a cyclonic eddy in the Gulf of California during the summer. *Deep Sea Research Part I: Oceanographic Research Papers*, *75*, 39–51. https://doi.org/10.1016/J.DSR.2013.01.009

Schmid, M. S., Cowen, R. K., Robinson, K., Luo, J. Y., Briseño-Avena, C., & Sponaugle, S. (2020). Prey and predator overlap at the edge of a mesoscale eddy: fine-scale, in-situ distributions to

inform our understanding of oceanographic processes. *Scientific Reports*, *10*(1). https://doi.org/10.1038/s41598-020-57879-x

Selph, K. E., Swalethorp, R., Stukel, M. R., Kelly, T. B., Knapp, A. N., Fleming, K., Hernandez, T., Landry, M. R., & Campbell, L. (2022). Phytoplankton community composition and biomass in the oligotrophic Gulf of Mexico. *Journal of Plankton Research*, *44*(5), 618–637. https://doi.org/10.1093/plankt/fbab006

Shih, Y. Y., Hung, C. C., Gong, G. C., Chung, W. C., Wang, Y. H., Lee, I. H., Chen, K. S., Ho, C. Y., & Hong, Y. (2015). Enhanced Particulate Organic Carbon Export at Eddy Edges in the Oligotrophic Western North Pacific Ocean. *PLOS ONE*, *10*(7), e0131538. https://doi.org/10.1371/JOURNAL.PONE.0131538

Shropshire, T. A., Morey, S. L., Chassignet, E. P., Karnauskas, M., Coles, V. J., Malca, E., Laiz-Carrión, R., Fiksen, Ø., Reglero, P., Shiroza, A., Quintanilla Hervas, J. M., Gerard, T., Lamkin, J. T., Stukel, M. R., & Dolan, J. (2022). Trade-offs between risks of predation and starvation in larvae make the shelf break an optimal spawning location for Atlantic bluefin tuna. *Journal of Plankton Research*, *44*(5), 782–798. https://doi.org/10.1093/plankt/fbab041

Silsbe, G. M., Behrenfeld, M. J., Halsey, K. H., Milligan, A. J., & Westberry, T. K. (2016). The CAFE model: A net production model for global ocean phytoplankton. *Global Biogeochemical Cycles*, *30*(12), 1756–1777. https://doi.org/10.1002/2016GB005521

Stukel, M. R., Landry, M. R., Benitez-Nelson, C. R., & Goericke, R. (2011). Trophic cycling and carbon export relationships in the California current ecosystem. *Limnology and Oceanography*, *56*(5), 1866–1878. https://doi.org/10.4319/lo.2011.56.5.1866

Toner, M., Kirwan, J. D., Poje, A. C., Kantha, L. H., Müller-Karger, F. E., & Jones, C. K. R. T. (2003). Chlorophyll dispersal by eddy-eddy interactions in the Gulf of Mexico. *Journal of Geophysical Research: Oceans*, *108*(4). https://doi.org/10.1029/2002jc001499

Vukovich, F. M. (2007). Climatology of Ocean Features in the Gulf of Mexico Using Satellite Remote Sensing Data. *Journal of Physical Oceanography*, *37*(3), 689–707. https://doi.org/10.1175/JPO2989.1

Wang, L., Huang, B., Laws, E. A., Zhou, K., Liu, X., Xie, Y., & Dai, M. (2018). Anticyclonic Eddy Edge Effects on Phytoplankton Communities and Particle Export in the Northern South China Sea. *Journal of Geophysical Research: Oceans*, *123*(11), 7632–7650. https://doi.org/10.1029/2017JC013623

Weisberg, R. H., Li, Z., & Muller-Karger, F. (2001). West Florida shelf response to local wind forcing: April 1998. *Journal of Geophysical Research: Oceans*, *106*(C12), 31239–31262. https://doi.org/10.1029/2000jc000529

Weisberg, R. H., & Liu, Y. (2017). On the Loop Current Penetration into the Gulf of Mexico. *Journal of Geophysical Research: Oceans*, *122*(12), 9679–9694. https://doi.org/10.1002/2017JC013330

Wormuth, J. H., Ressler, P. H., Cady, R. B., Harris, E. J., Ressler, P. H., Cady, R. B., & Harris, E. J. (2000). Zooplankton and Micronekton in Cyclones and Anticyclones in the Northeast Gulf of Mexico. *Gulf of Mexico Science*, *18*(1). https://doi.org/10.18785/goms.1801.03

Zhang, Z., & Qiu, B. (2018). Evolution of Submesoscale Ageostrophic Motions Through the Life Cycle of Oceanic Mesoscale Eddies. *Geophysical Research Letters*, *45*(21), 11,847-11,855. https://doi.org/10.1029/2018GL080399

Zhu, Y., & Liang, X. (2022). Characteristics of Eulerian mesoscale eddies in the Gulf of Mexico. *Frontiers in Marine Science*, *9*. https://doi.org/10.3389/fmars.2022.1087060